Molecular and Cellular Endocrinology 478 (2018) 17–31

Contents lists available at ScienceDirect

Molecular and Cellular Endocrinology

journal homepage: www.elsevier.com/locate/mce

NRG1 signalling regulates the establishment of Sertoli cell stock in the mouse testis

Elodie P. Gregoire[a], Isabelle Stevant[b], Anne-Amandine Chassot[a], Luc Martin[a], Simon Lachambre[a], Magali Mondin[a], Dirk G. de Rooij[c], Serge Nef[b], Marie-Christine Chaboissier[a,*]

[a] Université Côte d'Azur, CNRS, Inserm, iBV, France
[b] Department of Genetic Medicine and Development, Faculty of Medicine, University of Geneva, Switzerland
[c] Reproductive Biology Group, Division of Developmental Biology, Department of Biology, Faculty of Science, Utrecht University, Utrecht 3584 CH, the Netherlands

ARTICLE INFO

Keywords:
Testis
Nrg1
Progenitor cells
Proliferation
Hypoplasia

ABSTRACT

Testis differentiation requires high levels of proliferation of progenitor cells that give rise to two cell lineages forming the testis, the Sertoli and the Leydig cells. Hence defective cell cycling leads to testicular dysgenesis that has profound effects on androgen production and fertility. The growth factor NRG1 has been implicated in adult Leydig cell proliferation, but a potential function in the fetal testis has not been analysed to date. Here we show that *Nrg1* and its receptors *ErbB2/3* are already expressed in early gonadal development. Using tissue-specific deletion, we further demonstrate that *Nrg1* is required in a dose-dependent manner to induce proliferation of Sertoli progenitor cells and then differentiated Sertoli cells. As a result of reduced numbers of Sertoli cells, *Nrg1* knockout mice display a delay in testis differentiation and defects in sex cord partitioning. Taken together *Nrg1* signalling is essential for the establishment of the stock of Sertoli cells and thus required to prevent testicular hypoplasia.

1. Introduction

During embryogenesis, androgens produced by the testis are critical regulators of Wolffian ducts that give rise to male reproductive genitalia and male traits (Fluck et al., 2011; Shima and Morohashi, 2017). The synthesis of androgens requires two cell types: in fetal Leydig cells, cholesterol is converted into androstenedione that in turn is transformed into androgens in Sertoli cells (Shima et al., 2013). Both cell types originate from proliferating progenitor cells located in the coelomic epithelium (Schmahl et al., 2000). Proliferation of these progenitors occurs at low levels prior to sex determination and is under the control of *Six1/4*, as well as the insulin and WNT signalling pathways (Fujimoto et al., 2013; Pitetti et al., 2013; Chassot et al., 2012). After ingression into the male gonad, progenitor cells differentiate into fetal Leydig cells or Sertoli cells, a process that requires the expression of the sex-determining gene *Sry* and its target *Sox9* (Karl and Capel, 1998; Sekido and Lovell-Badge, 2008; Chaboissier et al., 2004). Additional proliferation of progenitor cells is then stimulated by FGF9, a growth factor secreted by the Sertoli cells (Schmahl et al., 2004). At 12.5 d*pc* in the mouse, proliferation in the coelomic epithelium returns to a basal level and progenitor cell invasion into the testis stops (Schmahl et al., 2000). Thus, the basal stock of Sertoli cells is yet established and its number determines the testicular size. Consequently, defects in progenitor cell proliferation leads to testicular dysgenesis (Schmahl and Capel, 2003). The identification of the signalling pathways underlying progenitor cell expansion is therefore crucial to better understand the occurrence of this pathology.

As testis differentiation proceeds, vascular endothelial cells migrating from the mesonephros and across the gonad promotes testis cord partitioning and assembly of the coelomic vessel at the surface of the gonad (Coveney et al., 2008; Combes et al., 2009). The development of sex cords is completed by deposition of a basement membrane by the smooth muscle like peritubular myoid cells (Tung et al., 1984).

After birth, the fetal Leydig cells are replaced by adult Leydig cells that produce all the enzymes required for androgen synthesis (Mendis-Handagama et al., 1987). Their number increases concomitantly with the level of LH (Luteinizing hormone) and this in turn leads to the expression of Neuregulin1 (NRG1), a transmembrane protein belonging to the epidermal growth factor family (Umehara et al., 2016). In addition to its role in adult Leydig cell proliferation, NRG1 also promotes spermatogonial proliferation in postnatal testes (Umehara et al., 2016; Zhang et al., 2011). Interestingly, *Nrg1* is expressed in the interstitial

Abbreviations: dpc, days post-coitum; dpp, days post-partum; LH, Luteinizing Hormone

* Corresponding author. Centre de biochimie, iBV, Université Côte d'Azur, 28, avenue de Valrose, 06108, Nice, France.
E-mail address: chaboiss@unice.fr (M.-C. Chaboissier).

https://doi.org/10.1016/j.mce.2018.07.004
Received 17 November 2017; Received in revised form 31 May 2018; Accepted 8 July 2018
Available online 21 July 2018
0303-7207/

cells of the embryonic testis from 12.5 d*pc* onwards (Jameson et al., 2012), but its role during testicular morphogenesis has remained elusive. Here we assess the contribution of *Nrg1* in testis development by analysing the consequences of *Nrg1* conditional ablation in XY embryonic gonads.

2. Materials and methods

2.1. Mouse strains and genotyping

All experiments were carried out in compliance with the relevant institutional and French animal welfare laws, guidelines and policies and have been approved by the French ethics committee and Ministry of Education and Research (APAFIS#3772-2016012215521604v3). All mouse lines were kept on a mixed 129/C57Bl6/J background. *Wt1-Cre*$^{Tg/+}$; *Nrg1*$^{fl/fl}$ or *Wt1-CreER*$^{T2/+}$; *Nrg1*$^{fl/fl}$ and controls (*Nrg1*$^{+/+}$, *Nrg1*$^{fl/+}$ *or Nrg1*$^{fl/fl}$) were obtained by crossing *Nrg1*$^{fl/fl}$ females with *Wt1-Cre*$^{Tg/+}$ or *Wt1-CreER*$^{T2/+}$ males and then *Nrg1*$^{fl/fl}$ or *Nrg1*$^{fl/+}$ females with *Wt1-Cre*$^{Tg/+}$; *Nrg1*$^{fl/+}$ or *Wt1-CreER*$^{T2/+}$; *Nrg1*$^{fl/+}$ (Zhou et al., 2008; Li et al., 2002). *ErbB2*$^{fl/fl}$ were mated with *ErbB3*$^{fl/fl}$ mice to obtain *ErbB2*$^{fl/fl}$; *ErbB3*$^{fl/fl}$ and then the *Wt1-CreER*$^{T2/+}$ was added by a cross-breeding scheme similar to that described above in order to obtain *Wt1-CreER*$^{T2/+}$; *ErbB2*$^{fl/fl}$; *ErbB3*$^{fl/fl}$ mice (Zhou et al., 2008; Garratt et al., 2000; Sheean et al., 2014). *Wt1-Cre*$^{Tg/+}$; *Nrg1*$^{fl/fl}$; *Rspo1*$^{+/-}$ mice were bred by crossing *Wt1-Cre*$^{Tg/+}$; *Nrg1*$^{fl/fl}$ females with *Rspo1*$^{-/-}$ males and next *Nrg1*$^{fl/+}$; *Rspo1*$^{+/-}$ females with *Wt1-Cre*$^{Tg/+}$; *Nrg1*$^{fl/+}$; *Rspo1*$^{+/-}$ males (Chassot et al., 2008). *Wt1-Cre*$^{Tg/+}$; *Nrg1*$^{fl/fl}$; *Rspo1*$^{-/-}$ mice were generated by crossing *Nrg1*$^{fl/fl}$; *Rspo1*$^{+/-}$ females with *Wt1-Cre*$^{Tg/+}$; *Nrg1*$^{fl/fl}$; *Rspo1*$^{+/-}$ males. Activation of the Cre recombinase in *Wt1-CreER*$^{T2/+}$; *Nrg1*$^{fl/fl}$ and *Wt1-CreER*$^{T2/+}$; *ErbB2*$^{fl/fl}$; *ErbB3*$^{fl/fl}$ females was carried out by oral gavage to pregnant females with 4 mg of tamoxifen (Sigma-Aldrich) dissolved in 90% corn oil (Sigma-Aldrich) and 10% ethanol, per 20 g of body weight. The stage of tamoxifen administration is noted in the corresponding figure legend. Embryos were collected from timed matings. The presence of a vaginal plug in the morning was used to indicate mating and was designated as 0.5 d*pc*. Embryos were staged by counting the number of tail somites (ts) with 8 ts corresponding to 10.5 d*pc* and 18 ts to 11.5 d*pc* (Hacker et al., 1995). Genotyping was performed using DNA extracted from tail tips or ear biopsies of mice and performed as described in (Zhou et al., 2008; Li et al., 2002; Garratt et al., 2000; Sheean et al., 2014; Chassot et al., 2008). Fertility tests were performed using 4-6 months-old *Wt1-Cre*$^{Tg/+}$; *Nrg1*$^{fl/fl}$ males mated with *Nrg1*$^{fl/fl}$ females.

2.2. Histological analysis

Testes were fixed in Bouin solution overnight and embedded in paraffin. Five µm thick sections were stained with Periodic-Acid-Schiff and analysed using a MZ9.5 (Leica) microscope coupled with a DHC490 (Leica) camera and application suite V3.3.0 (Leica) software and processed with Adobe Photoshop. Macroscopic views were performed with a MZ16 (Leica) microscope coupled with a DHC490 (Leica) camera and application suite V3.3.0 (Leica) software and processed with Adobe Photoshop.

2.3. In-situ hybridization

Tissue samples were fixed in 4% paraformaldehyde in PBS overnight at 4 °C, embedded in paraffin and hybridizations were carried out essentially as described in (Chassot et al., 2008). *Nrg1* digoxigenin–labelled riboprobe was synthetized using 576 bp matching sequence (Fig. 1E). *ErbB2* riboprobe was generated by PCR amplification of gonadal cDNA using the FErbB2: 5′-tggtccagcctgagccatgg-3′ and RErbB2: 5′-acttgtccaaagggtctcg-3′ primers and cloning in the pCR®II-TOPO® vectors (Invitrogen life technologies). *ErbB3* riboprobe was kindly provided by Michael Wegner. Post-hybridization washes were performed in 100 mM maleic acid pH7.5, 150 mM NaCl, 0.1% (v/v) tween-20 (MABT). Imaging was performed using a MZ9.5 (Leica) microscope coupled with a DHC490 (Leica) camera and application suite V3.3.0 (Leica) software and processed with Adobe Photoshop.

2.4. Immunofluorescence analyses on sections

Tissue samples were fixed in 4% paraformaldehyde overnight at 4 °C and embedded in paraffin. Microtome sections of five µm thickness were used for immunofluorescence experiments as described in (Chassot et al., 2008). The dilutions of primary antibodies are reported in Table S5. Slides were counterstained with DAPI diluted in the mounting medium at 10 µg/ml (Vectashield, Vector Laboratories) to visualize the nuclei. They were analysed with a motorized Axio ImagerZ1 microscope (Zeiss) coupled with an Axiocam Mrm camera (Zeiss) and processed with Axiovision LE (Zeiss) and Adobe Photoshop.

2.5. Wholemount immunohistochemistry

Gonads were fixed in 4% paraformaldehyde for 1 h and incubated in 30% Methanol - 3.75% H_2O_2. Nonspecific epitopes were blocked using 5% milk powder for 5 h. The samples were then incubated with anti-PECAM1 (1:50) and visualized with 0.05% DAB - 0.015% H_2O_2 according to standard procedures. The analysis was performed using a MZ16 (Leica) microscope coupled with a DHC490 (Leica) camera and application suite V3.3.0 (Leica) software and processed with Adobe Photoshop.

2.6. Wholemount immunofluorescence

Gonads were fixed in 4% paraformaldehyde overnight at 4 °C and were incubated in washing/blocking solution (1% Donkey serum, 1% Triton X-100, 3% BSA in PBS). After incubation with AMH (1:200, sc6886, Santa Cruz Biotechnology) and CD144 antibodies (1:200, 550548, BD Pharmigen) for 48 h and overnight in washing/blocking solution, secondary antibodies were incubated overnight (1:500, Life Technologies). Following overnight in washing/blocking solution, samples were dehydrated in methanol (25%–100% in PBS) and were clarified in 1:1 Methanol: BABB solution (1:2 Benzyl Alcohol, 1.09626.1000, Millipore; Benzyl Benzoate, B9550, Sigma) and in BABB solution. Imaging was performed on a LSM 880 inverted Axio Observer confocal microscope (Carl Zeiss Microscopy GmbH, Jena, Germany) using a Plan Apo 10X dry NA 0.45. Images were acquired using an Argon LASER at 488 nm and a DPSS 561 nm. Fluorescence emission was detected on a descanned GaAsp PMT, and z acquisitions were performed using a piezo z-drive. Images were processed with Imaris 9.1 Bitplane.

2.7. Reverse transcription PCR analysis

Individual gonads were dissected from the mesonephros in PBS at 13.5 d*pc* and immediately frozen at −80 °C. RNA was extracted using the PureLink™ RNA Mini kit (Ambion), and reverse transcribed using the MMLV reverse transcriptase (28025-013, Invitrogen). The primers used were *Nrg1* 5′-cgagtgcttcatggtgaagg-3′ and 5′-cgaccaccaacagggcgata-3’. Thirty cycles of PCR were sufficient to visualize the PCR products. The band of 120 bp was extracted using the QIAquick PCR Purification Kit (28104, Qiagen) and sequenced by Eurofins Genomics.

2.8. Quantification of cells

Paraffin sections of five µm thickness were processed for immunostaining experiments using the MKI67 antibody or and DAPI to identify proliferative cells and nuclei respectively. Additional proliferation analyses were performed on the same sections by way of 5-Bromo-2′-deoxy-Uridine labelling and detection using an appropriate

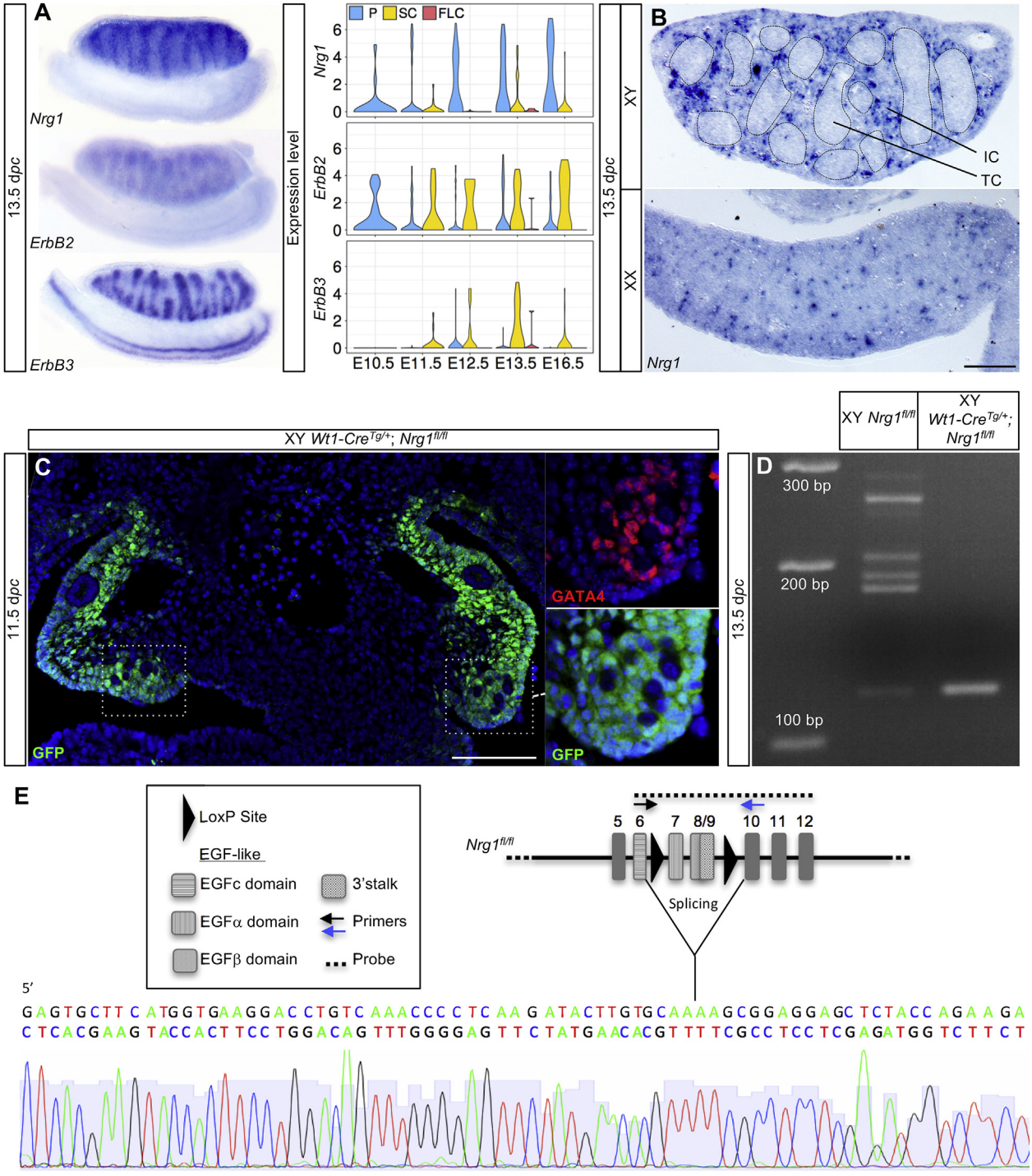

Fig. 1. Expression of *Nrg1* and the receptors *ErbB2* and *ErbB3* in developing testes and *Nrg1* knock-down strategy (A) Whole-mount *in situ* hybridization at 13.5 d*pc* using a *Nrg1* probe (highlighted in E), *ErbB2* and *ErbB3* probes (described in Materials and Methods). Violin graphs representing the single-cell expression profiles of *Nrg1*, *ErbB2* and *ErbB3* from 10.5 d*pc* to 16.5 d*pc* in the different NR5A1^{+} somatic cell population of the fetal testis. This profiling analysis includes 401 individual *Nr5a1*$^{+}$ transcriptomes from Progenitors (P), Sertoli Cells (SC) and Fetal Leydig Cells (FLC). The width of the violin indicates frequency at that expression level. **(B)** *In situ* hybridization using a *Nrg1* probe (highlighted in E) at 13.5 d*pc* on XY and XX gonadal sections. Scale bar: 100 µm. IC: Interstitial Cells, TC: Testis Cord. **(C)** Immunolocalization of GATA4 (red) and GFP (green) in XY *Wt1-Cre*$^{Tg/+}$; *Nrg1*$^{fl/fl}$ gonads at 11.5 d*pc* (17 tail somites). *Gfp* is encoded by the *Wt1-Cre* transgene and GFP identifies the cell expressing the Cre recombinase. A white box frames the gonads and the hand-right insets show a magnification of the right gonad. Nuclei are stained in blue with DAPI. Scale bar: 1000µm. **(D)** RT PCR analysis demonstrating the deletion of the EGF-like domain of *Nrg1* in the targeted alleles in XY *Wt1-Cre*$^{Tg/+}$; *Nrg1*$^{fl/fl}$ gonads. The transcripts containing this domain were readily detected in the XY *Nrg1*$^{fl/fl}$ gonads at 13.5 d*pc*. In both genotypes, a band of 120 bp was visualized and results from a splicing between exons flanking the EGF-like domain of *Nrg1* in **(E)**. **(E)** Sequencing of the 120 bp isoform visualized in (D) was performed with primers indicated with the blue arrow. Schematic representation of *Nrg1* allele containing the *LoxP* sites (black arrowheads). Arrows represent the primers used in RT PCR analysis and the dotted line represents the *in situ* probe. (For interpretation of the references to colour in this figure legend, the reader is referred to the Web version of this article.)

kit (cat 11 296 736 001, Roche). The gonads were collected 4 h after BrdU intraperitoneal injection and were visualized with NR5A1 (SF1) or GATA4 immunolocalization at 11.25 d*pc* (NR5A1: 1:1000, kindly provided by Ken-ichirou Morohashi (Morohashi et al., 1993), and GATA4: 1:200) and Sertoli cells with WT1 at 14.5 d*pc*. Apoptosis/TUNEL analysis was performed with the In Situ Cell Death Detection kit, TMR red (cat 11 684 795 910, Roche). MKI67, BrdU or TUNEL-positive cells were counted manually with Fiji/ImageJ (NIH) software and DAPI- positive cells were counted using the Measure Function in Volocity (PerkinElmer) software. At 14.5 d*pc,* cell types were identified using CDH1, WT1 (or SOX9), NR2F2 or NR5A1 as a germ cell marker, Sertoli cell marker, interstitial cell marker or Leydig cell marker in addition to DAPI to calculate the percentage of each type of cells. The number of CDH1, WT1 (SOX9), NR2F2 and NR5A1 positive cells were counted manually with Fiji/ImageJ (NIH) software. The number of total cells (DAPI positive) were counted using Measure Function in Fiji/ImageJ (NIH) or in Volocity (PerkinElmer) softwares (Figs. 2, 5 and 7). Then the percentage of antibody-positive cells versus total cells (DAPI positive) was determined. For each genotype (~9–12 pictures), the mean ± S.E.M. of these percentages were calculated and reported on a graph after statistical analysis (for details, see paragraph Statistical Analysis below).

2.9. Quantitative PCR analysis

Individual testis with mesonephros were dissected in PBS from 11 d*pc* to 11.75 d*pc* embryos and immediately frozen at −80 °C. RNA was extracted using the PureLink™ RNA Mini kit (Ambion), and reverse

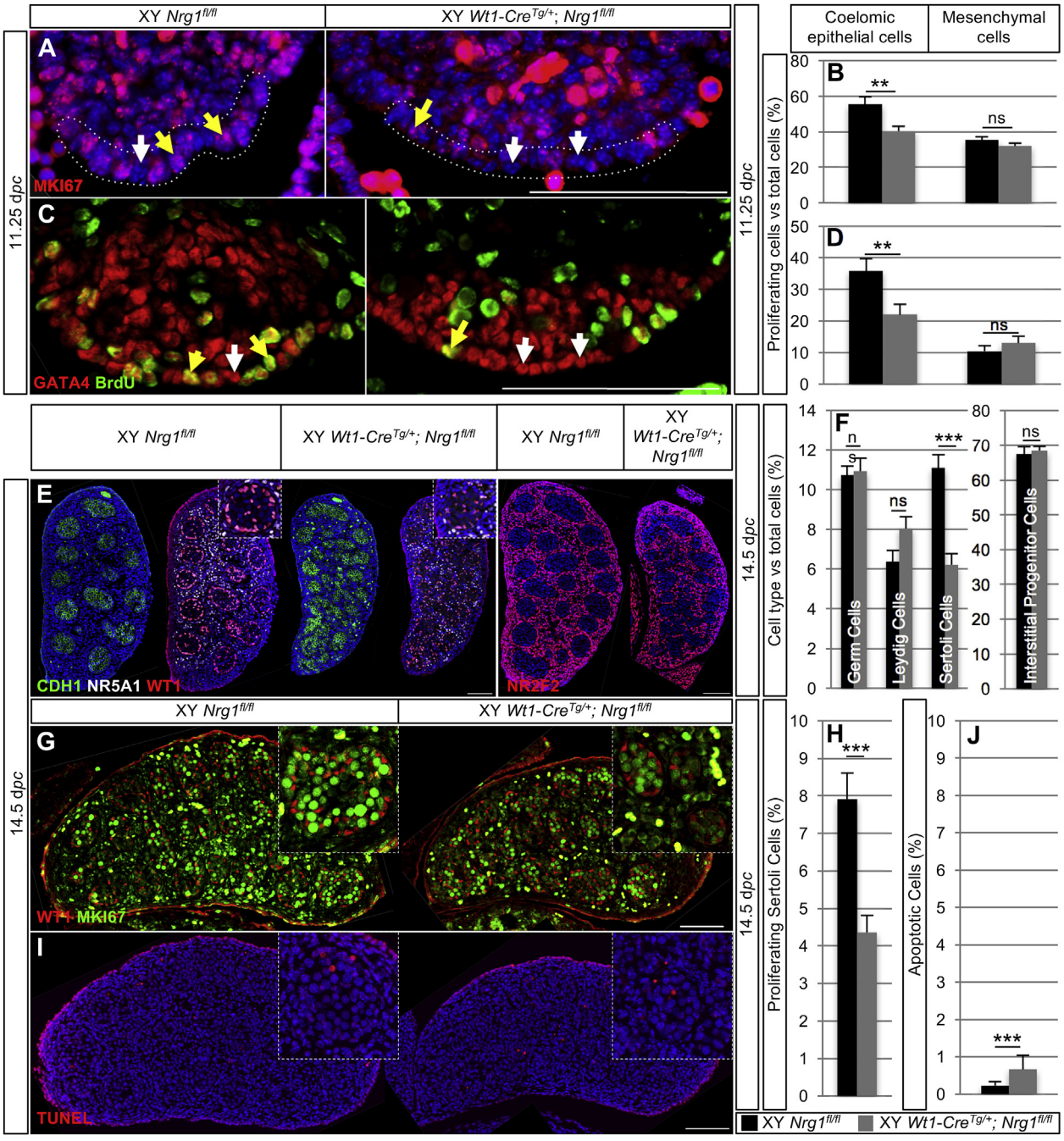

(caption on next page)

Fig. 2. Reduction of progenitor cells proliferation and in Sertoli cell numbers in XY *Wt1-Cre*$^{Tg/+}$; *Nrg1*$^{fl/fl}$ gonads. (A) MKI67 (red) immunostaining in XY *Wt1-Cre*$^{Tg/+}$; *Nrg1*$^{fl/fl}$ and in XY control gonads at 11.25 d*pc* (15–17 ts). Nuclei are stained in blue with DAPI. Scale bar: 100 µm. The coelomic region is delimited by the white dashes (first raw of cells on the surface of the gonad, yellow arrows for proliferating cells and white arrows for non-proliferating cells). **(B)** Quantification of the proliferating MKI67-positive coelomic epithelial cells versus the total cells in the coelomic epithelium (n = 3 embryos per genotype) and quantification of the proliferating mesenchymal cells versus total mesenchymal cells in XY *Wt1-Cre*$^{Tg/+}$; *Nrg1*$^{fl/fl}$ (grey histogram; n = 3 embryos, 1 gonad per embryo) and in XY control gonads (black histogram; n = 4). Quantification was performed using 4 sections spaced more than 30 µm apart in each gonad. ns: non-significant. **: p value < 0.01. **(C)** GATA4 (red) and BrdU (green) immunostaining in XY *Wt1-Cre*$^{Tg/+}$; *Nrg1*$^{fl/fl}$ and in XY control gonads at 11.25 d*pc* (14–17 ts). Scale bar: 100 µm. The coelomic region is the first row of GATA4-positive cells on the surface of the gonad. Yellow arrows indicate proliferating cells and white arrows show non-proliferating cells). **(D)** Quantification of the proliferating BrdU-positive coelomic epithelial cells versus the total cells in the coelomic epithelium (n = 3 embryos per genotype) and quantification of the proliferating mesenchymal cells versus total mesenchymal cells in XY *Wt1-Cre*$^{Tg/+}$; *Nrg1*$^{fl/fl}$ (grey histogram; n = 3 embryos per genotype) and in XY control gonads (black histogram; n = 3). Quantification was performed using 3 sections spaced more than 30 µm apart in each gonad. ns: non-significant. **: p value < 0.01. **(E)** CDH1 (green), NR5A1 (white), WT1 (red) and NR2F2 (red) immuno-detections in XY *Wt1-Cre*$^{Tg/+}$; *Nrg1*$^{fl/fl}$ and in XY control gonads at 14.5 d*pc* used to count germ cells, Leydig cells, Sertoli cells and interstitial progenitor cells respectively. In XY *Nrg1*$^{fl/fl}$ and XY *Wt1-Cre*$^{Tg/+}$; *Nrg1*$^{fl/fl}$ WT1-positive cells of coelomic epithelium were not counted. Nuclei are stained in blue with DAPI. Scale bar: 100 µm. **(F)** Quantification of germ cells, Leydig cells, Sertoli cells and interstitial progenitor cells at 14.5 d*pc* in XY *Wt1-Cre*$^{Tg/+}$; *Nrg1*$^{fl/fl}$ (grey histogram; n = 4 for germ cells, Leydig cells, Sertoli cells; n = 3 for interstitial progenitor cells) versus XY control gonads (black histogram; n = 3). Quantification was performed using 3 sections spaced more than 30 µm apart in each gonad/embryo. ns: non-significant. ***: p value < 0.0001. Bars represent mean ± s.e.m. **(G)**. MKI67 (green) and WT1 (red) immuno-detections in XY *Wt1-Cre*$^{Tg/+}$; *Nrg1*$^{fl/fl}$ and in XY control gonads at 14.5 d*pc* used to count proliferating Sertoli cells. In XY *Nrg1*$^{fl/fl}$ and XY *Wt1-Cre*$^{Tg/+}$; *Nrg1*$^{fl/fl}$ WT1-positive cells of coelomic epithelium were not counted. Scale bar: 100 µm. **(H)** Quantification of proliferating Sertoli cells at 14.5 d*pc* in XY *Wt1-Cre*$^{Tg/+}$; *Nrg1*$^{fl/fl}$ (grey histogram; n = 3) versus XY control gonads (black histogram; n = 3). Quantification was performed using 3 sections spaced more than 30 µm apart in each gonad/embryo. ***: p value < 0.0001. Bars represent mean ± s.e.m. **(I)**. TUNEL (red) immuno-detections in XY *Wt1-Cre*$^{Tg/+}$; *Nrg1*$^{fl/fl}$ and in XY control gonads at 14.5 d*pc* used to count apoptotic cells. In XY *Nrg1*$^{fl/fl}$ and XY *Wt1-Cre*$^{Tg/+}$; *Nrg1*$^{fl/fl}$ TUNEL-positive cells of coelomic epithelium were not counted. Scale bar: 100 µm. **(J)** Quantification of apoptotic Sertoli cells at 14.5 d*pc* in XY *Wt1-Cre*$^{Tg/+}$; *Nrg1*$^{fl/fl}$ (grey histogram; n = 3) versus XY control gonads (black histogram; n = 3). Quantification was performed using 3 sections spaced more than 30 µm apart in each gonad/embryo. ***: p value < 0.0001. Bars represent mean ± s.e.m. (For interpretation of the references to colour in this figure legend, the reader is referred to the Web version of this article.)

transcribed using the MMLV reverse transcriptase (28025-013, Invitrogen). Quantitative RT-PCR (QPCR) was performed using the LightCycler Taqman Master kit (Roche). Primers and probes were designed by the Roche Assay Design Center (http://qpcr.probefinder.com/organism.jsp). *Sry*: 5′-agcctcatcggagggcta-3′ and 5′-aggcaactgcaggctgtaaa-3′ (Probe: 82). *Nr5a1*: 5′-cgtaaactgcgcacaggag-3′ and 5′-gtagattggttcagggaagg-3′ (Probe: 105). *Fgf9*: 5′-tgcaggactggatttcatttag-3′ and 5′-ccaggcccactgctatactg-3′ (Probe: 60). *ErbB3*: 5′-cgagaactgcacccaagg-3′ and 5′-tctgcttggcctaaacagtct-3′ (Probe: 93). QPCR was performed on cDNA from one testis-mesonephros and compared with a standard curve. Relative expression levels of each gene were quantified in the same run and normalized on the levels of *Nr5a1* relative expression. QPCR were repeated at least twice. The number of gonads per genotype is mentioned in the figure legends. Details of statistical analyses are in the paragraph below.

2.10. Statistical analysis

Data are shown as mean ± s.e.m.

All the data were analyzed by unpaired one-sided Student's *t*-test using Microsoft Excel (Redmond, WA, USA). Asterisks highlight the pertinent comparisons and indicate levels of significance: *: p value < 0.05, **: p value < 0.01 and ***: p value < 0.0001.

2.11. Single-cell RNA sequencing

CD-1 female mice were bred with heterozygous *Tg(Nr5a1-GFP)* transgenic male mice (Stallings et al., 2002). On the relevant days of gestation (10.5 d*pc*, 11.5 d*pc*, 12.5 d*pc*, 13.5 d*pc* and 16.5 d*pc*), Nr5a1-GFP$^+$ male gonads were collected, and cell dissociated. GFP$^+$ somatic cells were sorted by FACS and single-cells were processed using the C1 Single-Cell Auto Prep System (Fluidigm). Reverse-transcription and pre-amplification of the single-cell cDNAs were achieved within the IFC chip using the SMARTer Ultra Low RNA kit for Illumina (Clontech) according to the C1 protocol. RNA-sequencing libraries of the single-cell cDNA were prepared using the Illumina Nextera XT DNA Sample Preparation kit using the modified protocol described in the C1 documentation. Libraries were multiplexed distributing the embryonic stages on all the lanes and sequenced as 100 bp paired-end reads using the Illumina HiSEQ 2000 platform at a minimum depth of 10 million reads per cell.

The computations were performed at the Vital-IT (http://www.vital-it.ch) Center for high-performance computing of the SIB Swiss Institute of Bioinformatics. FastQ files were mapped with GemTools (version 1.7.1) to the mouse reference genome (GRCm38. p3) and the genome annotation (version M4) downloaded from GENCODE. Bam files were generated using SamTools (version 0.1.19). Demultiplexing, mapping, read count per gene, per exon, and RPKM (Reads Per Kilobase of exon per Million reads mapped) were computed with an in-house pipeline.

Classification of the cells was performed with hierarchical clustering on principal component (HCPC, R package FactoMineR) on the highly variable genes. Biological relevance of the classification was confirmed by looking at the expression of marker genes of each known somatic cell types. Among the 400 NR5A1$^+$ cells, 290 were classified as somatic progenitors, 100 as pre Sertoli and Sertoli cells and 7 as fetal Leydig cells. Graphics were generated with Ggplot2 and edited with Inkscape. Full material and methods of this experiment is described in (Stevant et al., 2018).

2.12. RNA sequencing analysis

Individual gonads without mesonephros were dissected in PBS from 13.5 d*pc* and immediately frozen at −80 °C. Eight gonads were pooled from XY *Nrg1*$^{fl/fl}$ or XY *Wt1-Cre*$^{Tg/+}$; *Nrg1*$^{fl/fl}$ and RNA was extracted using RNeasy® Micro Kit (74004, Qiagen). The experiment is carried out in quadruplet. RNA libraries were constructed using the Illumina TruSeq Stranded mRNA kit and sequenced using HiSeq 2500 at Eidgenössische Technische Hochschule Zürich (ETHZ, Zurich, Schweiz). Fastq sequences files were upload to the Galaxy server (https://usegalaxy.org) for further processing (Afgan et al., 2016). Sequences were pre-processed using FASTQ groomer, checked using Fastqc and trimmed to keep base between 15 and 68 with the Trim sequences tool. RNA-seq reads were aligned to the mouse genome GRCm38/mm10 using the TopHat software (Galaxy version 2.1.0) (Kim et al., 2013). Aligned reads were counted using HTSeq (Anders et al., 2015) with refGene annotation file downloaded from the UCSC genome browser website. Low expressed genes were discarded (when the sum of count reads for each gene in all samples were below 10 counts) and differential expression analysis was performed using the DESeq2 (version 1.14.0) (Love et al., 2014) with default settings. Heatmap were generated using the ComplexHeatmap package (Gu et al., 2016) of the

R software and GO enrichment analysis was processed using the ClueGO module of Cytoscape (Bindea et al., 2009; Shannon et al., 2003). RNA-seq data are available in the ArrayExpress database (http://www.ebi.ac.uk/arrayexpress) under access number E-MTAB-5772.

3. Results

3.1. Nrg1 and receptors ErbB are expressed in the embryonic testis

NRG1 belongs to a family of membrane glycoproteins including NRG2, NRG3 and NRG4 (Wolpowitz et al., 2000). The *Nrg1* gene encodes various isoforms generated through alternative start sites and splicing events and all isoforms harbour an EGF-like signalling domain (Meyer and Birchmeier, 1995; Meyer et al., 1997). We first analysed the pattern of expression of *Nrg1* using the transcriptome of 400 individual *Nr5a1*$^{+}$ cells at five different developmental stages of testicular differentiation (10.5, 11.5, 12.5, 13.5 and 16.5 d*pc*) (Stevant et al., 2018). We found that *Nrg1* is the most expressed gene of the *Nrg* gene family in the somatic cells in the testis (Fig. S1A). *Nrg1* is strongly expressed in somatic progenitor cells of the developing testis as early as 10.5 d*pc* and then until 16.5 d*pc* (Fig. 1A). Subsequently, *Nrg1* expression decreases when the cells differentiate either as Sertoli or Leydig cells. Consistent with the single-cell RNA sequencing data, *in situ* hybridizations highlighted *Nrg1* up-regulation in the interstitial cells at 13.5 d*pc*. By contrast, *Nrg1* is weakly expressed in ovaries at this stage ((Jameson et al., 2012) & Fig. 1A–B).

NRG1 has a high affinity for the two-tyrosine kinase receptors, ERBB3 and ERBB4. ERBB2 is devoid of the binding domain and must dimerize with ERBB3/4 to exert its kinase activity (Hynes and Lane, 2005). Our single cell RNA-Seq analysis reveals that *ErbB2* is expressed in somatic progenitor cells and at much higher levels in Sertoli cells. QPCR analysis also shows the expression of *ErbB3* at 11–11.25 d*pc* (Fig. S1D). Then *ErbB3* and *ErbB4* are up-regulated in Sertoli cells (Fig. 1A; Fig. S1B & (Naillat et al., 2014)). *Nrg1* shows a dynamic pattern of expression with a high level of expression in the progenitor cells during embryogenesis and a predominant expression in adult Leydig cells after birth, as reported previously (Umehara et al., 2016).

3.2. Nrg1 deletion impairs progenitor cells proliferation in developing testis

To investigate the role of *Nrg1* in testis development, we generated mutant mice lacking *Nrg1* in somatic cells of the gonads expressing *Wt1* (*Wt1-Cre*$^{Tg/+}$; *Nrg1*$^{fl/fl}$). We first assessed the gonadal expression of the *Wt1-Cre* at 11.5 d*pc,* which also encodes the green fluorescent protein (GFP) (Zhou et al., 2008). As expected, the *Wt1-Cre*$^{Tg/+}$ transgene was expressed in all somatic cells of the XY gonads as exemplified by GFP immunostainings (Fig. 1C). Next, we evaluated the efficiency of *Nrg1* ablation by *LoxP* sites recombination in the XY gonads. It is noteworthy that the *LoxP* sites have been inserted in the flanking regions of the EGF-like domain of *Nrg1*, thus deleting this receptor-binding domain upon recombination (Fig. 1E) (Li et al., 2002). RT-PCR analysis revealed that all *Nrg1* isoforms containing the EGF-like domain were eliminated in XY *Wt1-Cre*$^{Tg/+}$; *Nrg1*$^{fl/fl}$ gonads. One band of 120 bp was detected in the mutant and control gonads (Fig. 1D). Sequencing analyses of this band showed that the corresponding isoform(s) is (are) devoid of the EGF-like domain (Fig. 1E). We concluded that the signalling molecule NRG1 is efficiently inactivated in XY *Wt1-Cre*$^{Tg/+}$; *Nrg1*$^{fl/fl}$ gonads.

Nrg1 is a positive regulator of proliferation and differentiation (Li et al., 2002). Since *Nrg1* is expressed during early development when the testicular progenitors actively proliferate, we examined whether *Nrg1* is involved in this process. Quantification analysis of proliferative cells using immunostainings for MKI67 carried out at 11.25 d*pc* indicated a decrease in proliferation of 27.0% in *Wt1-Cre*$^{Tg/+}$; *Nrg1*$^{fl/fl}$ gonads in comparison to controls (Fig. 2A–B). This reduction was more conspicuous in the coelomic epithelial region than in the internal mesenchymal part of the gonads (Fig. 2A–B). We confirmed the reduction of proliferation of the coelomic epithelial cells in XY *Wt1-Cre*$^{Tg/+}$; *Nrg1*$^{fl/fl}$ gonads by using BrdU labelling assays. The BrdU is incorporated in the newly synthetized DNA in the cells progressing through the S-phase of the cell cycle. A reduction of 38.7% of progenitor cells that incorporated BrdU was estimated in *Wt1-Cre*$^{Tg/+}$; *Nrg1*$^{fl/fl}$ testis compared to controls (Fig. 2C–D). Altogether these data demonstrate that *Nrg1* is involved in progenitor cell proliferation in the developing testis.

3.3. Nrg1 deletion induces a reduction in Sertoli cells in a dose-dependent manner

Sertoli and interstitial cells including fetal Leydig cells arise from coelomic epithelial cells and a decrease in cell proliferation in this compartment is expected to also lead to a reduction of the number of these cells. Accordingly, XY *Wt1-Cre*$^{Tg/+}$; *Nrg1*$^{fl/fl}$ gonads displayed 43.9% fewer Sertoli cells, whereas interstitial cell, fetal Leydig cell and germ cell numbers were not significantly changed between mutant and controls (Figs. S2C and G; Fig. 2E-F). To address whether a deficit of proliferation of the differentiated Sertoli cells and/or an increase of their apoptosis also contributes in the reduced number of Sertoli cells, we estimated the number of proliferating MIK67-positive or apoptotic TUNEL-positive cells respectively at 14.5 d*pc* (Fig. 2G–J). This showed that the proliferation of the differentiated Sertoli cells is significantly reduced in XY *Wt1-Cre*$^{Tg/+}$; *Nrg1*$^{fl/fl}$ testes when compared to controls. We found that the deficit of proliferation was 44.9% (Fig. 2G–H). Whereas the number of apoptotic cells was increased in XY *Wt1-Cre*$^{Tg/+}$; *Nrg1*$^{fl/fl}$ gonads, there were only rare apoptotic cells with an average of 0.2% in control gonads and 0.7% in XY mutants. This indicates that the absence of *Nrg1* does not induce a sufficient level of apoptosis to explain a cell type deficit (Fig. 2I–J). Therefore, *Nrg1* is involved in the proliferation of the Sertoli cell lineage from the progenitor cells to the differentiated Sertoli cells during embryonic testis development.

To exclude any effect of *Wt1* heterozygosity caused by the use of the *Wt1-Cre* line (knock-in), we also analysed Sertoli cell numbers in XY *Wt1-Cre*$^{Tg/+}$ and wild-types at 14.5 d*pc* (n = 4 for transgenic and n = 3 for wild-type gonads; p = 0.53, Figs. S2A and E). Interestingly, in XY *Wt1-Cre*$^{Tg/+}$; *Nrg1*$^{fl/+}$ gonads, the heterozygous mutation of *Nrg1* revealed a haploinsufficient phenotype with a reduction of 25.2% of Sertoli cells (n = 4 mutant and control gonads; p = 0.001, Figs. S2B and F). Gene expression analysis was conducted using RNA sequencing in XY control and mutant gonads at 13.5 d*pc*. A gene ontology analysis indicated that misregulated genes in the mutant gonads have been shown to be involved in gonadal development (Fig. S3C). The heatmap based on the expression of genes in XY control and mutant gonads revealed that genes were less expressed in the XY *Wt1-Cre*$^{Tg/+}$; *Nrg1*$^{fl/fl}$ gonads (Fig. 3A). This was the case for genes expressed in Sertoli cells such as *Sox9*, *Sox8*, *Sox 10*, *Amh*, *Dhh*, *Wt1*. This reduced expression level was likely reflecting the reduced number of Sertoli cells in mutant gonads (Fig. S3B). Altogether these results show that *Nrg1* regulates the proliferation of Sertoli cell progenitors and this promotes the establishment of the stock of Sertoli cells in the embryonic testis.

3.4. Sertoli cell differentiation is delayed in absence of Nrg1

After ingression of Sertoli cell progenitors into the gonad, *Sry* becomes up-regulated from 10.5 d*pc*, peaks at 11.5 d*pc* and is down-regulated in differentiated Sertoli cells at 12.5 d*pc* (Hacker et al., 1995). *Sry* expression was assessed by qPCR experiments in control and mutant embryos at stages ranging between 11 and 11.75 d*pc,* as we have previously performed (Fig. 3A & (Nef et al., 2003)). In these experiments, we used *Nr5a1* as a control, since it is expressed in somatic cells expressing *Sry* (Sekido and Lovell-Badge, 2008). Analysis of control gonads showed the expected increase of *Sry* expression between 11 and

11.75 d*pc*. By contrast, expression of *Sry* was reduced in the XY *Wt1-Cre*$^{Tg/+}$; *Nrg1*$^{fl/fl}$ gonads in comparison to control testes between 11 and 11.25 d*pc* and reached a similar level of expression after 11.5 d*pc*. An extended time of expression was evident in immunofluorescence analysis and SRY-positive cells were readily detectable in XY *Wt1-Cre*$^{Tg/+}$; *Nrg1*$^{fl/fl}$ gonads in comparison with controls at 12.5 d*pc* (Fig. 3C) (Bradford et al., 2007). Following *Sry* expression, the Sertoli differentiate and synthetizes the growth factor FGF9, that in turn stimulates

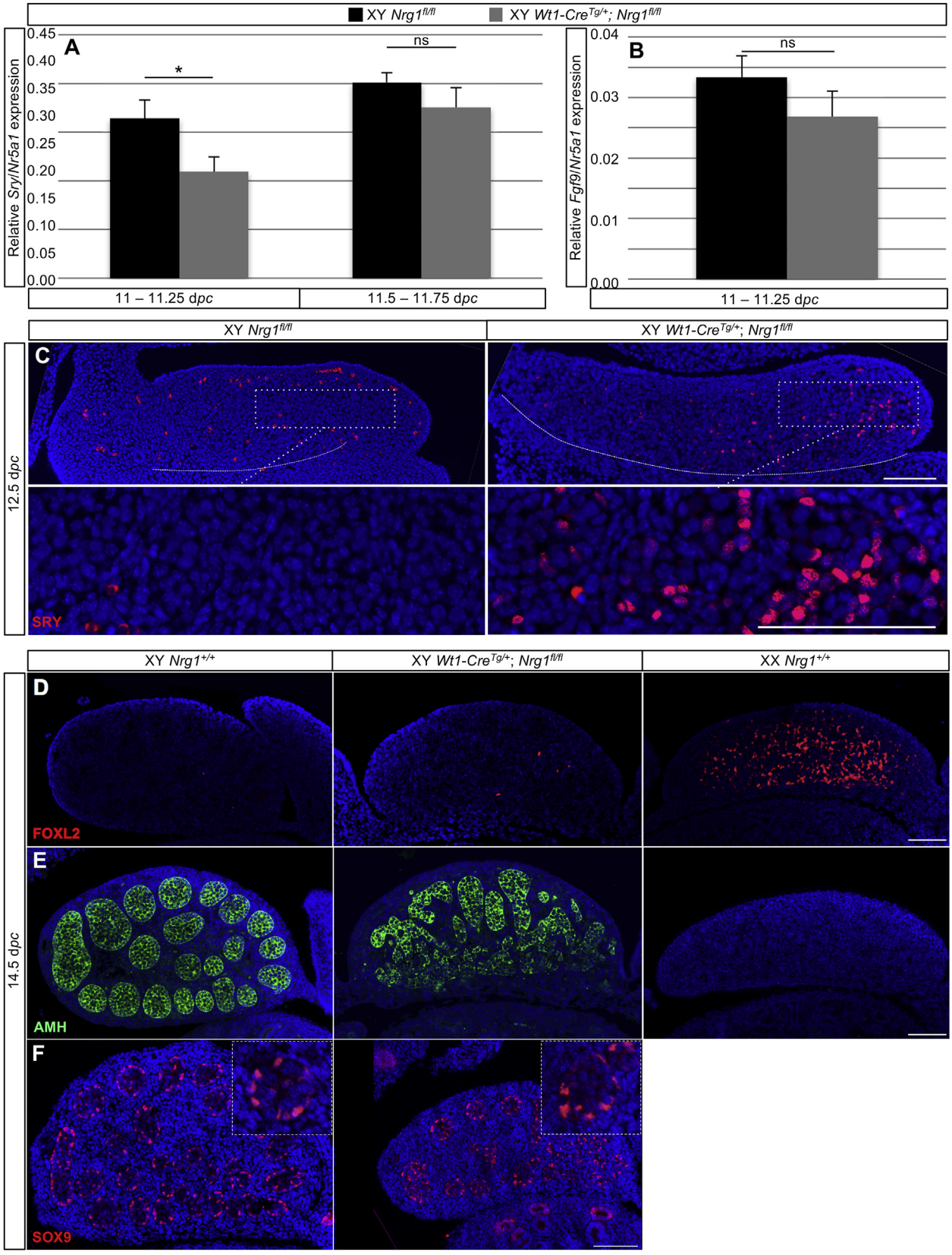

(caption on next page)

Fig. 3. Delayed *Sry* expression in XY *Wt1-Cre*$^{Tg/+}$; *Nrg1*$^{fl/fl}$ gonads does not induce sex reversal. (A) Quantitative RT PCR for *Sry* in the gonads and mesonephros at 11 d*pc* to 11.25 d*pc* (12–17 ts) and 11.5 d*pc* to 11.75 d*pc* (18–23 ts) in XY *Wt1-Cre*$^{Tg/+}$; *Nrg1*$^{fl/fl}$ gonads (grey histogram; n = 7 at 11–11.25 d*pc* and n = 4 at 11.5–11.75 d*pc*) versus the XY *Nrg1*$^{fl/fl}$ gonads (black histogram; n = 12 and n = 12). The level of relative expression of *Sry* is normalized with *Nr5a1,* which is expressed in somatic gonadal cells but not in mesonephros. ns: non-significant. *: p value < 0.05. Bars represent mean ± s.e.m. **(B)** Quantitative RT PCR for *Fgf9* in the gonads and mesonephros at 11 d*pc* to 11.25 d*pc* (12–17 ts) in XY *Wt1-Cre*$^{Tg/+}$; *Nrg1*$^{fl/fl}$ gonads (grey histogram; n = 7) versus the XY *Nrg1*$^{fl/fl}$ gonads (black histogram; n = 12). The level of relative expression of *Fgf9* is normalized with *Nr5a1,* which is expressed in somatic gonadal cells but not in mesonephros. ns: non-significant. Bars represent mean ± s.e.m. **(C)** SRY (red) immunostaining in XY *Wt1-Cre*$^{Tg/+}$; *Nrg1*$^{fl/fl}$ and in XY control gonads at 12.5 d*pc*. Nuclei are stained in blue with DAPI. The lower panel is a magnification of the area delimited by the white lines on the upper panel. Scale bar: 100 µm. **(D)** Immunolocalization of FOXL2 (granulosa cell marker; red), and **(E)** of AMH (Sertoli cell marker during embryogenesis; green) in XY *Wt1:Cre*$^{Tg/+}$; *Nrg1*$^{fl/fl}$, in XY and in XX control gonads at 14.5 d*pc*. Nuclei are stained in blue with DAPI. Scale bar: 100µm. **(F)** SOX9 (red) immunostaining in XY *Wt1-Cre*$^{Tg/+}$; *Nrg1*$^{fl/fl}$ and in XY control gonads at 14.5 d*pc*. Nuclei are stained in blue with DAPI. Scale bar: 100 µm. (For interpretation of the references to colour in this figure legend, the reader is referred to the Web version of this article.)

the proliferation of the progenitor cells. QPCR experiments indicate that the expression of *Fgf9* tends to be reduced although not significantly (Fig. 3B). This reduction is likely due to the lower numbers of Sertoli cells in XY *Wt1-Cre*$^{Tg/+}$; *Nrg1*$^{fl/fl}$ gonads and might contribute to the reduced level of proliferation of the progenitor cells.

Sry expression levels must reach a critical threshold between 11.0 and 11.25 d*pc* to induce testis differentiation (Hiramatsu et al., 2009) and if this threshold is not attained on time, male-to-female sex reversal can occur (Bullejos and Koopman, 2005). The observed retarded *Sry* expression in *Wt1-Cre*$^{Tg/+}$; *Nrg1*$^{fl/fl}$ embryos thus raised the question whether testis development maybe disrupted in this model potentially leading to expression of female-specific markers. Although a small increase of *FoxL2* expression was detected at 13.5 d*pc* (Fig. S3B), immunostaining of FOXL2 did not identify granulosa cells in XY mutant gonads in contrast to XX control ovaries at 14.5 d*pc* (Fig. 3D). Moreover, SOX9 and AMH (embryonic Sertoli cell markers)-positive cells were apparent in XY control and mutant embryos confirming that supporting progenitor cells were able to differentiate to Sertoli cells (Fig. 3E–F). Thus, the level of *Sry* expression was sufficient to permit male sex determination in XY *Wt1-Cre*$^{Tg/+}$; *Nrg1*$^{fl/fl}$ gonads. Taken together these observations demonstrate that ablation of *Nrg1* does not prevent Sertoli cell differentiation *per se* but delays their differentiation.

3.5. Defects in testis cord partitioning in absence of Nrg1

The immunolocalization of AMH revealed a disorganization of the Sertoli cells in the mutant testis, suggesting a disruption of sex cord formation (Fig. 3E & Movie S1 for the control and Movie S2 for the XY *Wt1-Cre*$^{Tg/+}$; *Nrg1*$^{fl/fl}$ gonad). At 14.5 d*pc,* co-immunostaining of LAMA1 (basal lamina deposited on sex cords) and CDH1 (germ cell marker) highlighted loop-like testis cords in longitudinal sections of control testes (Fig. 4A). In XY *Wt1-Cre*$^{Tg/+}$; *Nrg1*$^{fl/fl}$ gonads, LAMA1 deposits revealed the irregular structure of testis cords (Fig. 4A). A three-dimensional reconstruction of AMH immunostainings corroborated that the sex cords are disorganized in XY *Wt1-Cre*$^{Tg/+}$; *Nrg1*$^{fl/fl}$ testes at 13.5 d*pc* (Fig. 4B). Altogether, this indicates that ablation of *Nrg1* alters testis cord formation.

Supplementary video related to this article can be found at https://doi.org/10.1016/j.mce.2018.07.004.

The compartmentalization of the testis cords depends on endothelial cell migration from the mesonephros to the coelomic region (Coveney et al., 2008; Combes et al., 2009). At 13.5 d*pc*, PECAM1 (endothelial and germ cell marker) and CD144 (VE-Cadherin: a vascularization marker) immunostainings in control gonads revealed strings of connected endothelial cells forming vessels, located between the testis cords that contain Sertoli and germ cells (Fig. 4B&S4). In contrast, isolated endothelial cells were readily detectable in mutant gonads. These PECAM1-positive endothelial cells were identified by their elongated shape, whereas germ cells are round (Fig. S4). Interestingly, the sporadic endothelial cells were mostly located in the vicinity of the disorganized sex cords. Migration of endothelial cells is required for the coelomic vessel assembly. In controls and mutant testes, whole mount immunostainings of CD144 and PECAM1 showed that the coelomic vessel had formed indicating that endothelial cell migration was not severely impaired (Fig. 4B–C). It is noteworthy that these experiments using whole gonads also reveal that XY *Wt1-Cre*$^{Tg/+}$; *Nrg1*$^{fl/fl}$ gonads were smaller than controls at 13.5 d*pc*. Altogether these results show that *Nrg1* is involved in testicular morphogenesis.

In XY *Wt1-CreER*$^{T2/+}$; *ErbB2*$^{fl/fl}$; *ErbB3*$^{fl/fl}$ mutants, down-regulation of *ErbB2/3* was performed using the inducible *Wt1-CreER*$^{T2/+}$ recombinase (Zhou et al., 2008). We administered two doses of tamoxifen to pregnant females at 9.25 and 10.25 d*pc* allowing recombination of the *ErbB2/3*^{fl} alleles for ~24 h before the onset of testis morphogenesis (Liu et al., 2016). The disorganization of sex cords was visualized by LAMA1 immunostainings in mutants of the *ErbB2/3* receptors of NRG1 (Fig. S5A). This phenotype was associated with a 44.1% decrease in Sertoli cell numbers (Fig. 5A–B). These results confirmed that the NRG/ERBB signalling pathway is necessary for the establishment of the stock of Sertoli cells in the developing testis.

3.6. Nrg1 signalling is required at the time of sex determination

To assess the contribution of Sertoli cells in testis partitioning, we also used the inducible *Wt1-CreER*$^{T2/+}$ to induce down-regulation of *Nrg1* in a time-dependent manner by administration of tamoxifen at 9.25 and 10.25 d*pc*. We first evaluated the impact of the *Wt1-CreER*$^{T2/+}$ after tamoxifen treatment and found a non-significant reduction of the Sertoli cell numbers (4.7%; n = 5 for mutant and control gonads; p = 0.34, Figs. S2D and H). At 14.5 d*pc*, the number of Sertoli cells was decreased by 21.8% and LAMA1 immunostainings in XY *Wt1-CreER*$^{T2/+}$; *Nrg1*$^{fl/fl}$ gonads revealed a disorganization of the testis cords (Fig. 5C–D; S5B). When tamoxifen was administered at 11.25 and 11.75 d*pc,* the decrease in the number of Sertoli cells dropped to 14.8% and *Wt1-CreER*$^{T2/+}$; *Nrg1*$^{fl/fl}$ testes did not show structural defects as evidenced by the localization of the LAMA1 marker (Fig. 5E–F; S5C). This suggests that a reduction between 15% and 21% in the number of Sertoli cells was sufficient to alter testicular development in XY *Wt1-CreER*$^{T2/+}$; *Nrg1*$^{fl/fl}$ embryos.

3.7. Nrg1 ablation in developing testis leads to testicular hypoplasia

Next, to address the consequences of the reduced number in Sertoli cells on germ cell clustering in *Wt1-Cre*$^{Tg/+}$; *Nrg1*$^{fl/fl}$ embryos, we examined testes at birth. In neonates, the quiescent gonocytes were more abundant in the sex cords of the *Wt1-Cre*$^{Tg/+}$; *Nrg1*$^{fl/fl}$ testes with on average 4.0 gonocytes per tubule cross section (27 cross-sections in 2 sections) versus 1.5 in controls (43 cross-sections in 2 sections) (Fig. 6A). These observations indicate that the decreased Sertoli cell numbers results in shortage in amount in tubule space in *Wt1-Cre*$^{Tg/+}$; *Nrg1*$^{fl/fl}$ testes.

Further, XY quiescent gonocytes were localized between the tubules in the mutant testes and this was also observed at 14.5 d*pc* as evidenced

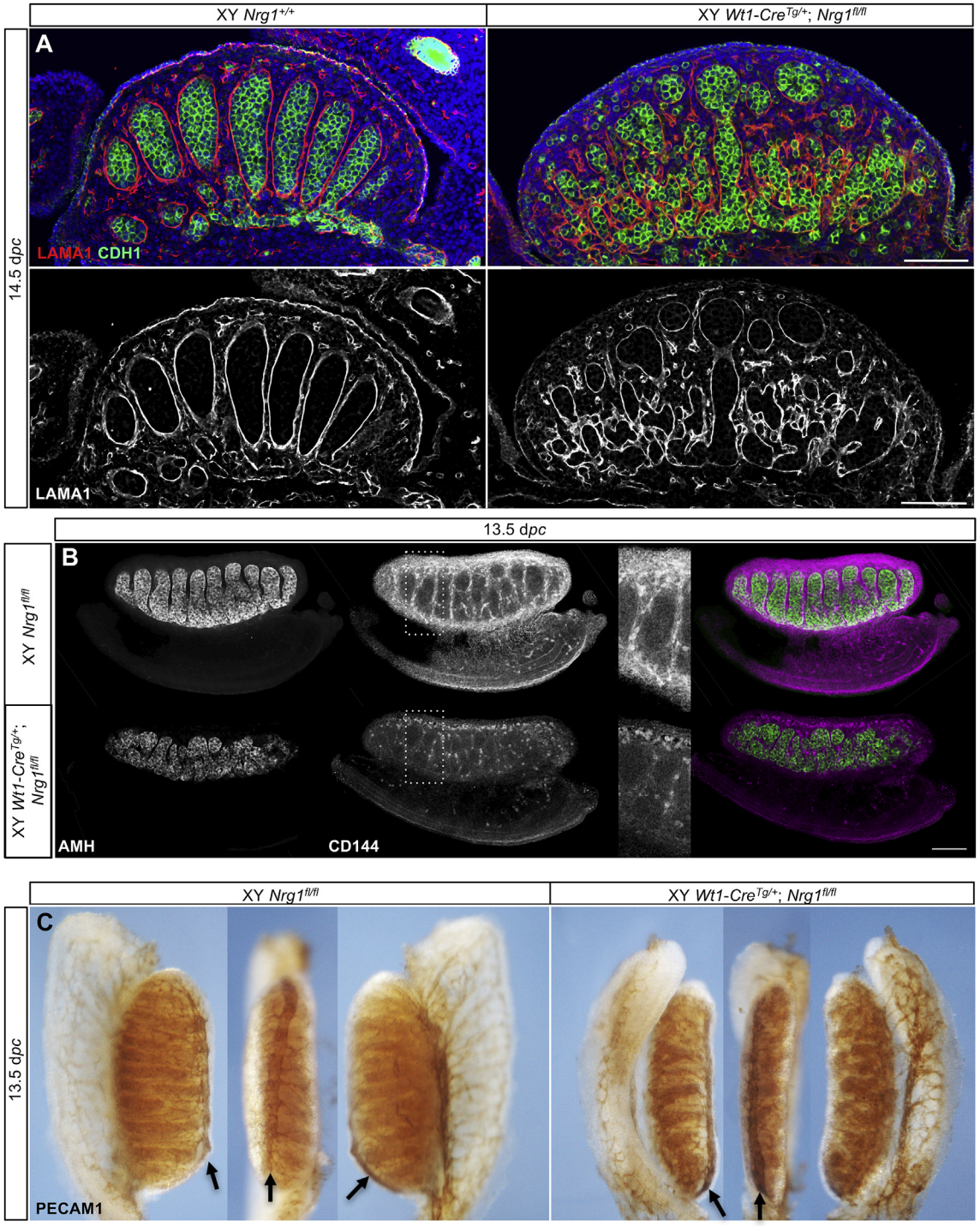

Fig. 4. Defects in testicular partitioning and vascularization in *Wt1-Cre*$^{Tg/+}$; *Nrg1*$^{fl/fl}$ testes. (A) LAMA1 (upper panel: red or lower panel: white) and CDH1 (green) immunolocalization in XY *Wt1-Cre*$^{Tg/+}$; *Nrg1*$^{fl/fl}$ and in XY control gonads at 14.5 d*pc*. Nuclei are stained in blue with DAPI. Scale bar: 100 µm. **(B)** Immunolocalization of AMH (left panel: white) and CD144 (middle panel: white) and AMH/CD144 (Left panel: green and purple respectively) in XY *Wt1-Cre*$^{Tg/+}$; *Nrg1*$^{fl/fl}$ and in XY control gonads at 13.5 d*pc*. The panel with the magnification is the area delimited by the white lines on the middle panel. Scale bar: 100 µm. **(C)** Immuno histochemistry of PECAM1 (endothelial and germ cell marker) in XY *Wt1-Cre*$^{Tg/+}$; *Nrg1*$^{fl/fl}$ and in XY control gonads at 13.5 d*pc*. Arrows show the coelomic vessel. (For interpretation of the references to colour in this figure legend, the reader is referred to the Web version of this article.)

by isolated DDX4 or CDH1-positive germ cells (Fig. 6A–B; Fig. 4A). The gonocytes within or outside the sex cords, expressed the pluripotency marker POU5F1 at 14.5 d*pc* indicating that they did not enter meiosis (Fig. S6). This also highlights that the reduced number of Sertoli cells are able to provide a favourable environment for XY gonocytes to become quiescent. Gonocytes resume spermatogenesis after birth and spermatogonia enter meiosis around 10–12 d*pp* during the first wave of spermatogenesis (de Rooij, 2001). At this stage, *Wt1-Cre*$^{Tg/+}$; *Nrg1*$^{fl/fl}$ testes were smaller and weighed 32,6% less than in controls thus highlighting hypoplasia of the mutant testes (Fig. 6C). In adult mice,

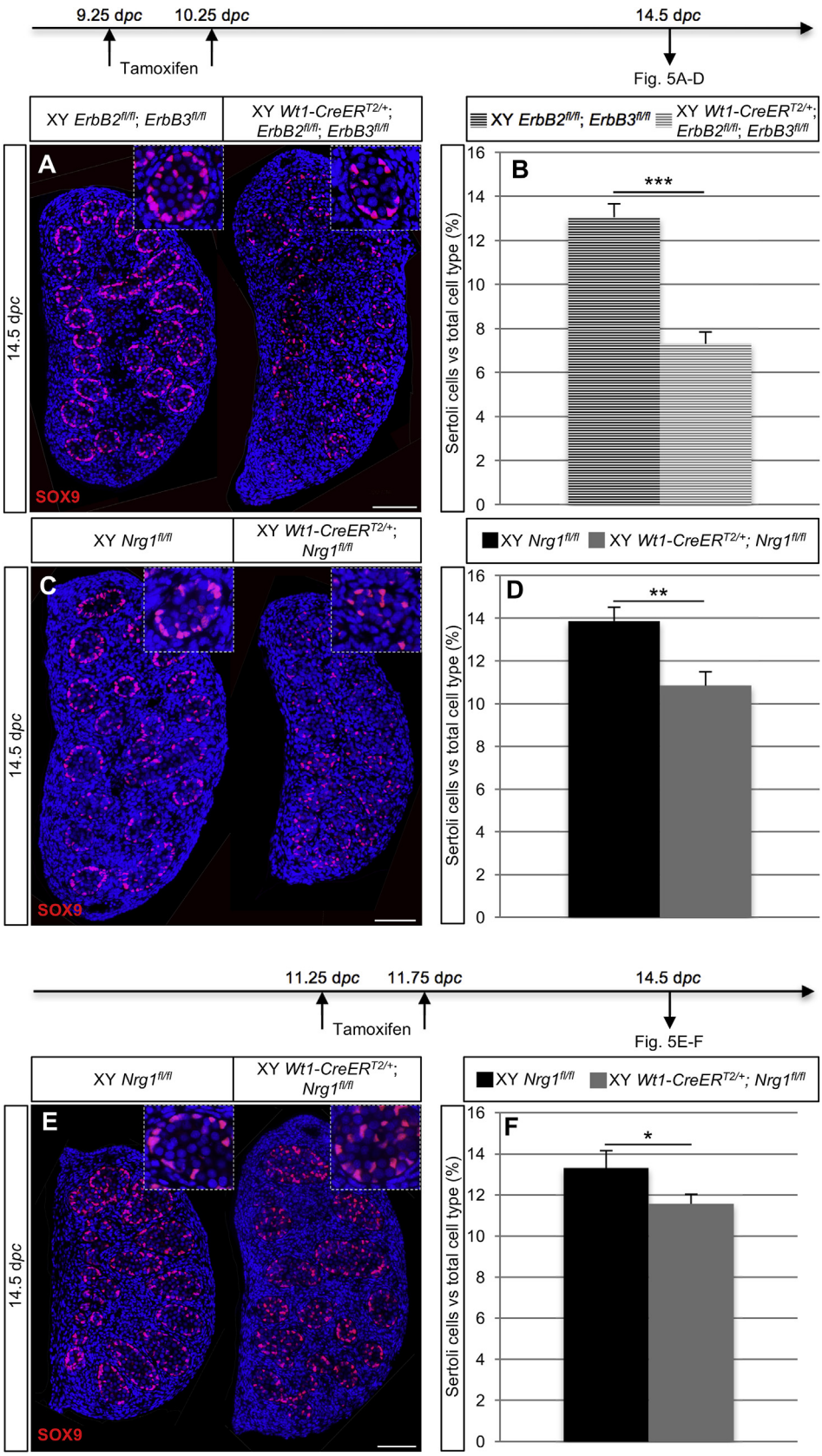

Fig. 5. *Nrg1/ErbB2/3* signalling mediates the establishment of Sertoli cells stock. 1-Reduction of Sertoli cell numbers in *ErbB2/3* mutant gonads. (A) SOX9 (red) immunolocalization in XY *Wt1-CreER*$^{T2/+}$; *ErbB2*$^{fl/fl}$; *ErbB3*$^{fl/fl}$ and in XY control gonads at 14.5 d*pc*. Nuclei are stained in blue with DAPI. Oral gavage was performed at 9.25 d*pc* and 10.25 d*pc*. Scale bar: 100 µm. **(B)** Quantification of Sertoli cells at 14.5 d*pc* in XY *Wt1-CreER*$^{T2/+}$; *ErbB2*$^{fl/fl}$; *ErbB3*$^{fl/fl}$ (grey stripe histogram; n = 3 embryos, one gonad per embryo) versus XY control gonads (black stripe histogram; n = 3). Quantification was performed using 3 to 6 sections spaced more than 30 µm apart in each gonad/embryo (A). ***: p value < 0.0001.

2-Variation in the number of Sertoli cells depends on *Nrg1* down-regulation time. (C) SOX9 (red) immunolocalization in XY *Wt1-CreER*$^{T2/+}$; *Nrg1*$^{fl/fl}$ and in XY control gonads at 14.5 d*pc*. Nuclei are stained in blue with DAPI. Oral gavage was performed at 9.25 d*pc* and 10.25 d*pc*. Scale bar: 100 µm. **(D)** Quantification of Sertoli cells at 14.5 d*pc* in XY *Wt1-CreER*$^{T2/+}$; *Nrg1*$^{fl/fl}$ (grey histogram; n = 4 embryo) versus XY control gonads (black histogram; n = 4). Quantification was performed using 3 sections spaced more than 30 µm apart in each gonad/embryo (C). **: p value < 0.01. **(E)** SOX9 (red) immunolocalization in XY *Wt1-CreER*$^{T2/+}$; *Nrg1*$^{fl/fl}$ and in XY control gonads at 14.5 d*pc*. Nuclei are stained in blue with DAPI. Oral gavage was performed at 11.25 d*pc* and 11.75 d*pc*. Scale bar: 100 µm. **(F)** Quantification of Sertoli cells at 14.5 d*pc* in XY *Wt1-CreER*$^{T2/+}$; *Nrg1*$^{fl/fl}$ (grey histogram; n = 4) versus XY control gonads (black histogram; n = 4). Quantification was performed using 3 sections spaced more than 30 µm apart in each gonad/embryo (E). *: p value < 0.05. Bars represent mean ± s.e.m. (For interpretation of the references to colour in this figure legend, the reader is referred to the Web version of this article.)

hypoplastic *Wt1-Cre*$^{Tg/+}$; *Nrg1*$^{fl/fl}$ testes could be due to a combination of developmental defects ((Fig. 6D) & our present results) and spermatogenesis defects as previously reported (Umehara et al., 2016; Zhang et al., 2011). Nevertheless, the *Wt1-Cre*$^{Tg/+}$; *Nrg1*$^{fl/fl}$ males were healthy, fertile and produced litters of normal size with 7.23 pups/female (± 2.8) compared with 6.73 pups/female (± 1.79) for *Nrg1*$^{fl/fl}$ male littermates (n = 13 and n = 11 *Nrg1*$^{fl/fl}$ plugged females per genotype). In agreement with their normal fertility, no obvious

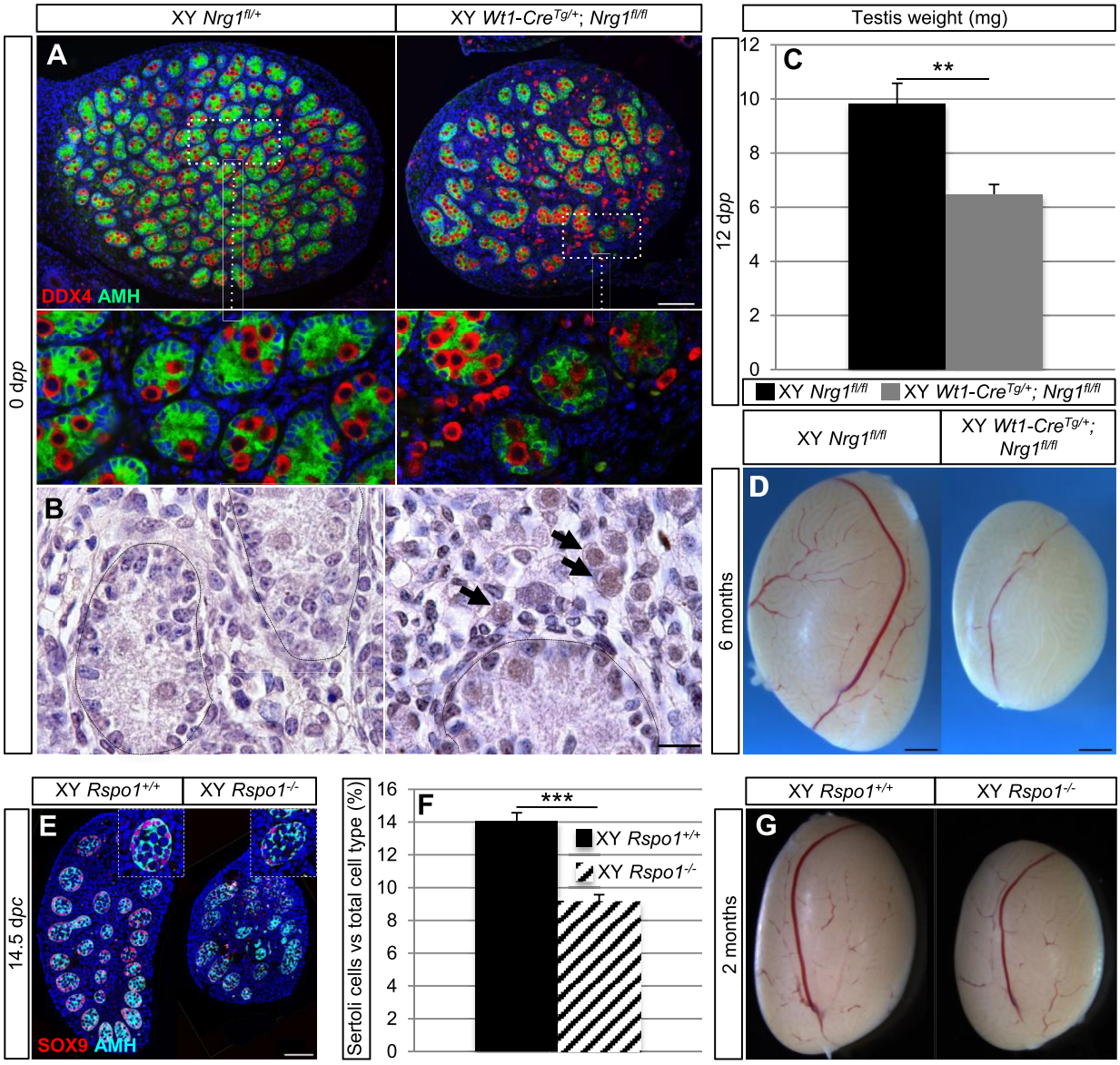

Fig. 6. XY *Wt1-Cre*$^{Tg/+}$; *Nrg1*$^{fl/fl}$ and *Rspo1*$^{-/-}$ mice exhibit hypoplastic testis. (A) DDX4/MVH (germ cell marker; red) and AMH (Sertoli cell marker; green) immunolocalization in XY *Wt1-Cre*$^{Tg/+}$; *Nrg1*$^{fl/fl}$ and in XY control gonads at 0 d*pp*. Magnification of the delimited area by white lines is shown in the lower panel. Nuclei are stained in blue with DAPI. Scale bar: 100 µm. **(B)** Periodic acid Schiff histological analysis of XY *Nrg1*$^{fl/+}$ and XY *Wt1-Cre*$^{Tg/+}$; *Nrg1*$^{fl/fl}$ testis at birth. Arrows indicate XY quiescent gonocytes localized between the tubules. Scale bar: 10 µm. **(C)** Weight of XY control (black histogram; n = 4), XY *Wt1-Cre*$^{Tg/+}$; *Nrg1*$^{fl/fl}$ testes (grey histogram; n = 5) at 12 d*pp*. **: p value < 0.01. Bars represent mean ± s.e.m. **(D)** Macroscopic view of XY *Wt1-Cre*$^{Tg/+}$; *Nrg1*$^{fl/fl}$ and XY control testis at 6 months. Scale bar: 1000µm. **(E)** SOX9 (red) and AMH (light blue) immunolocalization in XY *Rspo1*$^{-/-}$ and in XY control gonads at 14.5 d*pc*. Nuclei are stained in blue with DAPI. Scale bar: 100 µm. **(F)** Quantification of Sertoli cells at 14.5 d*pc* in XY *Rspo1*$^{-/-}$ (black stripe histogram; n = 3) versus XY *Rspo1*$^{+/+}$; *Nrg1*$^{+/+}$ control gonads from Fig. S2A (black histogram; n = 3). Quantification was performed using 3 sections spaced more than 30 µm apart in each gonad (E). Bars represent mean ± s.e.m. ***: p value < 0.0001. **(G)** Macroscopic view of XY *Rspo1*$^{-/-}$ and XY control testis at 2 months. (For interpretation of the references to colour in this figure legend, the reader is referred to the Web version of this article.)

structural or spermatogenesis abnormalities were observed in histological analyses (Fig. 7G).

3.8. Additive interaction of NRG1 and RSPO1 signalling on proliferation of the progenitor cells

We reported previously that *Rspo1* and *Wnt 4* also promote the proliferation of gonadal progenitors (Chassot et al., 2012). In order to decipher the interactions between the *Nrg1* and *Rspo1* signalling pathways, we took advantage of our single-cell RNA sequencing data to refine the expression pattern of *R-spondin* genes. *Rspo1* is expressed in the somatic progenitor cells in testes and becomes down-regulated when cells differentiate (Fig. S1C). In agreement with its role in progenitor proliferation, the number of Sertoli cells was reduced in *Rspo1*$^{-/-}$ testes in comparison with controls, and this led to testicular hypoplasia (Fig. 6E–G). When *Nrg1* and *Rspo1* mutations were combined in XY *Wt1-Cre*$^{Tg/+}$; *Nrg1*$^{fl/fl}$; *Rspo1*$^{-/-}$ gonads, the proliferation rates of coelomic epithelial cells (GATA4+) were highly reduced with an average of 48.5% in the double knock-out genital ridges compared to controls at 11.25 d*pc* (Fig. 7A–B). In addition, immunostaining for SOX9 revealed a stronger reduction of Sertoli cells (77.6%) in comparison with control gonads (Fig. 7C–D). Immunostaining using LAMA1 antibody revealed a stronger disorganization of the sex cords in XY *Wt1-Cre*$^{Tg/+}$; *Nrg1*$^{fl/fl}$; *Rspo1*$^{-/-}$ gonads in comparison with the single

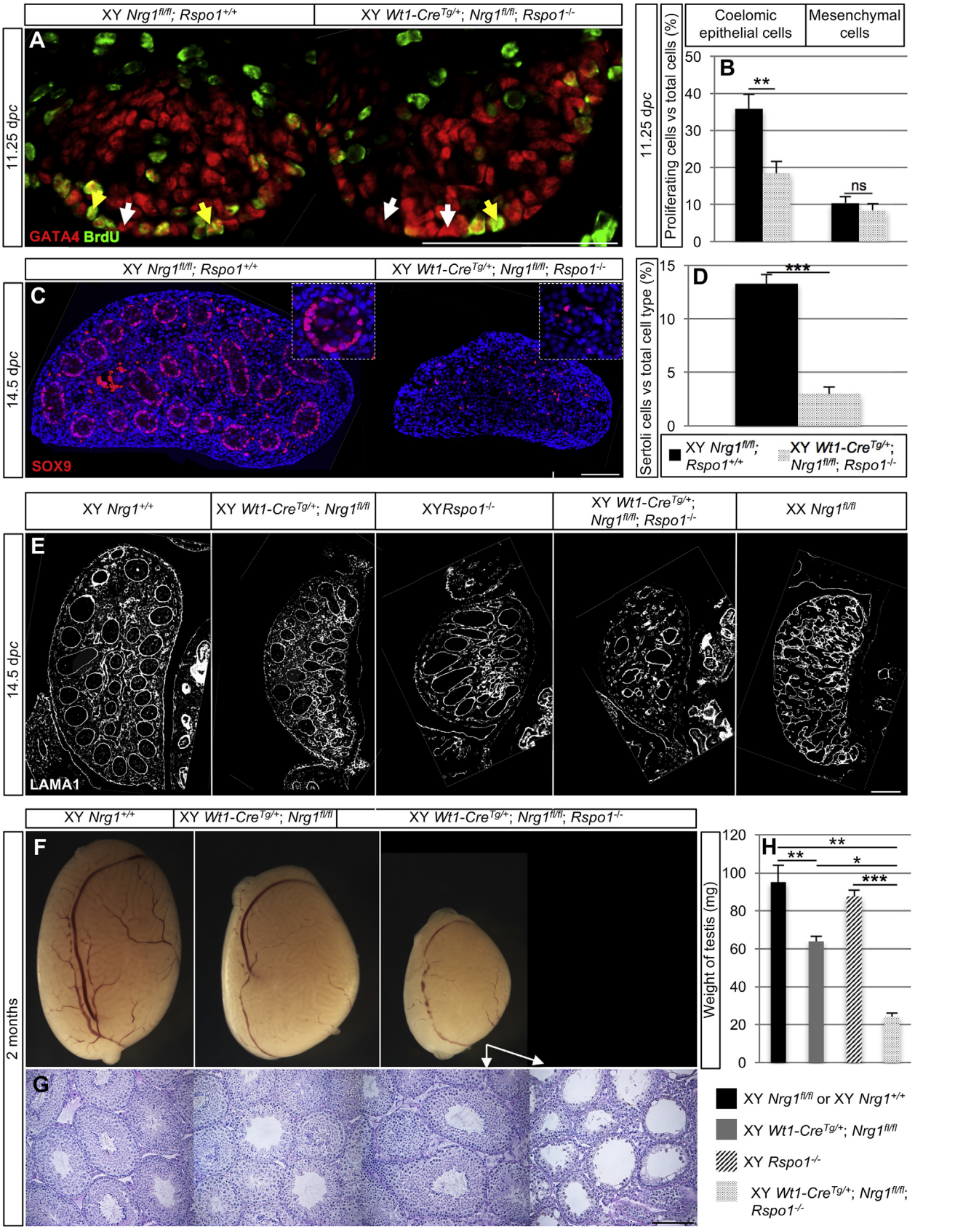

(caption on next page)

Fig. 7. Additional actions of *Rspo1* and *Nrg1* in testis development. (A) GATA4 (red) and BrdU (green) immunostaining in XY *Wt1-Cre*$^{Tg/+}$; *Nrg1*$^{fl/fl}$ and in XY control gonads at 11.25 d*pc* (14–17 ts). Scale bar: 100 µm. The coelomic region is the first row of GATA4-positive cells on the surface of the gonad, yellow arrows for proliferating cells and white arrows for non-proliferating cells). **(B)** Quantification of the proliferating BrdU-positive coelomic epithelial cells versus the total cells in the coelomic epithelium (n = 3 embryos per genotype) and quantification of the proliferating mesenchymal cells versus total mesenchymal cells in XY *Wt1-Cre*$^{Tg/+}$; *Nrg1*$^{fl/fl}$ (black spotted histogram; n = 3 embryos per genotype) and in XY control gonads (black histogram; n = 3). Quantification was performed using 3 sections spaced more than 30 µm apart in each gonad. ns: non-significant. **: p value < 0.01. **(C)** SOX9 (red) immunolocalization in XY *Wt1-Cre*$^{Tg/+}$; *Nrg1*$^{fl/fl}$; *Rspo1*$^{-/-}$ and XY control gonads at 14.5 d*pc*. Nuclei are stained in blue with DAPI. Scale bar: 100 µm. **(D)** Quantification of Sertoli cells at 14.5 d*pc* in XY *Nrg1*$^{fl/fl}$; *Rspo1*$^{+/+}$ control gonads from Fig. 5F (black histogram; n = 4) versus XY *Wt1-Cre*$^{Tg/+}$; *Nrg1*$^{fl/fl}$; *Rspo1*$^{-/-}$ (black spotted histogram; n = 3). Quantification was performed using 3 (black histogram) or 2 to 4 (black spotted histogram) sections spaced more than 30 µm apart in each gonad (D). Bars represent mean ± s.e.m. ***: p value < 0.0001. **(E)** LAMA1 (white) immunolocalization in XY control, XY *Wt1-Cre*$^{Tg/+}$; *Nrg1*$^{fl/fl}$, XY *Rspo1*$^{-/-}$, XY *Wt1-Cre*$^{Tg/+}$; *Nrg1*$^{fl/fl}$; *Rspo1*$^{-/-}$ and XX control gonads at 14.5 d*pc*. Scale bar: 100 µm. **(F)** Macroscopic views of XY control, XY *Wt1-Cre*$^{Tg/+}$; *Nrg1*$^{fl/fl}$ and XY *Wt1-Cre*$^{Tg/+}$; *Nrg1*$^{fl/fl}$; *Rspo1*$^{-/-}$ testis at 2 months. **(G)** Periodic acid Schiff histological analysis of XY control, XY *Wt1-Cre*$^{Tg/+}$; *Nrg1*$^{fl/fl}$ and XY *Wt1-Cre*$^{Tg/+}$; *Nrg1*$^{fl/fl}$; *Rspo1*$^{-/-}$ testis at 2 months. Scale bar: 200 µm. **(H)** Weight of XY control (n = 4), XY *Wt1-Cre*$^{Tg/+}$; *Nrg1*$^{fl/fl}$ (n = 3), XY *Rspo1*$^{-/-}$ (n = 3) and XY *Wt1-Cre*$^{Tg/+}$; *Nrg1*$^{fl/fl}$; *Rspo1*$^{-/-}$ (n = 3) testes at 2 months. *: p value < 0.05; **: p value < 0.01; ***: p value < 0.0001. Bars represent mean ± s.e.m. (For interpretation of the references to colour in this figure legend, the reader is referred to the Web version of this article.)

mutant *Wt1-Cre*$^{Tg/+}$; *Nrg1*$^{fl/fl}$ or *XY Rspo1*$^{-/-}$ testes at 14.5 d*pc* (Fig. 7E). These developmental defects lead to significantly more severe testicular hypoplasia of the double mutant males when compared to single mutant testes (Fig. 7F, H). Furthermore, XY *Wt1-Cre*$^{Tg/+}$; *Nrg1*$^{fl/fl}$; *Rspo1*$^{-/-}$ testes contain a proportion of seminiferous tubules exhibiting spermatogenesis defects that were not observed in the *Nrg1* or *Rspo1* single mutant testes (Fig. 7G). We conclude that the dramatic reduction in the number of Sertoli cells is associated with defects of the spermatogenesis as previously reported (Russell et al., 2002). Altogether, these data suggest that *Nrg1* and *Rspo1* have additive effects on the proliferation of progenitors of the Sertoli cells and thus on sex cords and seminiferous tubule formation.

4. Discussion

The first cellular process that is a hallmark of testicular differentiation is an increased level of somatic cell proliferation (Schmahl et al., 2000; Schmahl and Capel, 2003). It has been shown that FGF9 is required for proliferation of coelomic epithelial cells highly expressing NR5A1 from 11.2 d*pc*, which give rise to Sertoli and fetal Leydig cells (Schmahl et al., 2000, 2004). PDGFB stimulates a second wave of proliferation between 11.5 and 12.0 d*pc* (Brennan et al., 2002). At this latter stage, the cells express low levels of NR5A1 and divide to produce interstitial cells. This cellular expansion is spectacular since it enables a doubling in the testicular width every 24 h between 11.5 and 13.5 d*pc* in mice (Nel-Themaat et al., 2009). Our results show that NRG1 signalling is involved in progenitor cell proliferation at 11.25 d*pc* and then in the proliferation of differentiated Sertoli cells. Together, this contributes to the increase in Sertoli cell numbers but not to the interstitial including fetal Leydig cell numbers. This implies that NRG1 signalling is a newly identified mechanism required for the proliferation of the Sertoli cell lineage from the progenitors to the differentiated Sertoli cells and for the establishment of the stock of Sertoli cells necessary for the testis to reach a certain size.

Further, *Rspo1* and *Nrg1* signalling pathways have an additive effect. Both genes are expressed in the progenitor cells at 10.5 d*pc* and promote their proliferation in the coelomic region ((Chassot et al., 2012) & present results). The combined deletion of *Rspo1* and *Nrg1* induces a more dramatic phenotype in *Wt1-Cre*$^{Tg/+}$; *Nrg1*$^{fl/fl}$; *Rspo1*$^{-/-}$ testes with a severe hypoplasia of the testis. However, some Sertoli cells are still able to differentiate in the double mutant testes, suggesting that the deletion of *Nrg1* and *Rspo1* might be compensated for by other members of the same family. Indeed, we found that *Rspo3* and *Nrg4* are also expressed in the developing testis although at lower levels (Figs. S1A and C).

In addition to the growth of the testis, the migration of endothelial cells and the interstitial cells reorganization demarcate the cord forming domains initiating sex cords morphogenesis (Coveney et al., 2008; Combes et al., 2009). In the *Nrg1* mutant gonads, scattered endothelial cells were located in the vicinity of abnormal sex cords. This suggests that some defects in vascularization favour abnormal testis morphogenesis in embryos. We cannot exclude that *Nrg1* has a direct effect on endothelial cells. However this seems unlikely given that the receptors of NRG1 are not highly expressed in endothelial cells (Jameson et al., 2012). Although the process of testis cord organization was delayed at 14.5 d*pc*, it was complete at birth, reinforcing that *Nrg1* ablation triggers an overall delay in the differentiation of the embryonic testis. Moreover, examination of the male genitalia did not reveal abnormalities, suggesting that the reduced number of Sertoli cells did not impair androgen synthesis required for Wolffian duct differentiation during embryogenesis.

NRG1 interacts with the tyrosine kinase receptors ERBB3 and ERBB4 and their co-receptor ERBB2 (Falls, 2003). This interaction involves the extracellular EGF-like domain and thus elicits NRG/ERBB signalling. In our experimental settings, we used a conditional deletion of the EGF-like domain (Li et al., 2002). However, we found transcripts devoid of three exons encoding the EGF-like domain. The function of this (ese) potential isoform(s) has (have) not been reported to date. Given that these transcripts were present in the control and mutant gonads, the phenotypes on testicular proliferation and developmental defects are not associated with these potential isoforms, but rather due to down-regulation of the NRG/ERBB pathway. Here we show that the down-regulation of *ErbB2/3* induces a shortage in Sertoli cells and testicular disorganization at 14.5 d*pc,* supporting that NRG1 acts through these receptors during testis differentiation. The role of *ErbB4* in testis has been studied using a conditional loss-of-function mutation in Sertoli cells from 15 d*pc* (Naillat et al., 2014; Lecureuil et al., 2002). The *Amh-Cre*$^{Tg/+}$; *ErbB4*$^{fl/fl}$ mice exhibit testicular atrophy suggesting that *Nrg/ErbB* signalling remains involved in cell proliferation during the late development of the testes. In addition, *ErbB4*-negative Sertoli cells keep some embryonic characteristics such as production of testosterone that normally becomes Leydig cell specific in the adult testis implying a delay in Sertoli cell maturation. Furthermore adhesion defects between Sertoli and germ cells promote decreased sperm production and compromised fertility (Naillat et al., 2014). It is noteworthy that down-regulation of *Nrg1* in postnatal Sertoli cells impairs spermatogonial proliferation and meiosis entry (Zhang et al., 2011), whereas the elimination of *Nrg1* in our model does not impair spermatogenesis and fertility. The structural differences of both *Nrg1* knockout alleles may account for this discrepancy. Indeed in our model, three exons encoding the EGF-like domain are eliminated (Li et al., 2002), whereas one exon is only deleted in the model reported in (Zhang et al., 2011). It is possible that the remaining part of the EGF-like domain acts as a dominant negative mutation preventing any kind of complementation by other NRG ligands and therefore leads to a more dramatic phenotype during spermatogenesis. Recently, it has been found that *Nrg1* is expressed in adult Leydig cells and promotes adult Leydig cell proliferation (Umehara et al., 2016). Moreover, deletion of *Nrg1* eliminating the whole EGF-like domain in adult Leydig cells induces testosterone deficits leading to spermatogenesis defects and

impaired sexual behaviour. Subsequently, these mutant males are subfertile. Given that the *Wt1-Cre*$^{Tg/+}$; *Nrg1*$^{fl/fl}$ males are normally fertile, this may suggest that the early deletion of *Nrg1* allowed compensation by the expression of other NRG and thus a proper functioning of adult Leydig cells.

This previous analysis focused on the role of NRG1 in adult Leydig cells proliferation (Umehara et al., 2016). Here we show that NRG1 regulates the proliferation of progenitor cells and Sertoli cells and its loss leads to a deficit of the Sertoli cell number during embryogenesis. This demonstrates that NRG1 is an important activator for the proliferation of different testicular cell types during testis morphogenesis and after birth.

Funding

This work was supported by grants from the Fondation ARC, Agence Nationale de la Recherche (ANR_ARGONADS&ANR-11-LABX-0028-01) and SNSF N°31003A_173070 (to S.N.).

Acknowledgements

We thank Dr Carmen Birchmeier, Max Delbrück Center for Molecular Medicine (Berlin, Germany) for providing us with *Nrg1flox/flox,* ErbB2flox/flox and ErbB3flox/flox mice. We are grateful to Marie-Cécile De Cian, Isabelle Gillot, Aitana Perea-Gomez and Nainoa Richardson for critical reading of the manuscript and to Manuel Mark (IGBMC, University of Strasbourg) for his expertise in the histological analysis of testis. We are thankful to Ken-ichirou Morohashi (Fukuoka, Japan), Dagmar Wilhelm (University of Melbourne) and Michael Wegner (University of Erlangen) for the NR5A1 and SRY antibodies and *ErbB3* probe respectively.

Appendix A. Supplementary data

Supplementary data related to this article can be found at https://doi.org/10.1016/j.mce.2018.07.004.

References

Afgan, E., Baker, D., van den Beek, M., Blankenberg, D., Bouvier, D., Cech, M., Chilton, J., Clements, D., Coraor, N., Eberhard, C., Gruning, B., Guerler, A., Hillman-Jackson, J., Von Kuster, G., Rasche, E., Soranzo, N., Turaga, N., Taylor, J., Nekrutenko, A., Goecks, J., 2016. The Galaxy platform for accessible, reproducible and collaborative biomedical analyses: 2016 update. Nucleic Acids Res. 44, W3–W10.

Anders, S., Pyl, P.T., Huber, W., 2015. HTSeq–a Python framework to work with high-throughput sequencing data. Bioinformatics 31, 166–169.

Bindea, G., Mlecnik, B., Hackl, H., Charoentong, P., Tosolini, M., Kirilovsky, A., Fridman, W.H., Pages, F., Trajanoski, Z., Galon, J., 2009. ClueGO: a Cytoscape plug-in to decipher functionally grouped gene ontology and pathway annotation networks. Bioinformatics 25, 1091–1093.

Bradford, S.T., Wilhelm, D., Koopman, P., 2007. Comparative analysis of anti-mouse SRY antibodies. Sex Dev 1, 305–310.

Brennan, J., Karl, J., Capel, B., 2002. Divergent vascular mechanisms downstream of Sry establish the arterial system in the XY gonad. Dev. Biol. 244, 418–428.

Bullejos, M., Koopman, P., 2005. Delayed Sry and Sox9 expression in developing mouse gonads underlies B6-Y(DOM) sex reversal. Dev. Biol. 278, 473–481.

Chaboissier, M.C., Kobayashi, A., Vidal, V.I., Lutzkendorf, S., van de Kant, H.J., Wegner, M., de Rooij, D.G., Behringer, R.R., Schedl, A., 2004. Functional analysis of Sox8 and Sox9 during sex determination in the mouse. Development 131, 1891–1901.

Chassot, A.A., Ranc, F., Gregoire, E.P., Roepers-Gajadien, H.L., Taketo, M.M., Camerino, G., de Rooij, D.G., Schedl, A., Chaboissier, M.C., 2008. Activation of beta-catenin signaling by Rspo1 controls differentiation of the mammalian ovary. Hum. Mol. Genet. 17, 1264–1277.

Chassot, A.A., Bradford, S.T., Auguste, A., Gregoire, E.P., Pailhoux, E., de Rooij, D.G., Schedl, A., Chaboissier, M.C., 2012. WNT4 and RSPO1 together are required for cell proliferation in the early mouse gonad. Development 139, 4461–4472.

Combes, A.N., Wilhelm, D., Davidson, T., Dejana, E., Harley, V., Sinclair, A., Koopman, P., 2009. Endothelial cell migration directs testis cord formation. Dev. Biol. 326, 112–120.

Coveney, D., Cool, J., Oliver, T., Capel, B., 2008. Four-dimensional analysis of vascularization during primary development of an organ, the gonad. Proc. Natl. Acad. Sci. U. S. A. 105, 7212–7217.

de Rooij, D.G., 2001. Proliferation and differentiation of spermatogonial stem cells. Reproduction 121, 347–354.

Falls, D.L., 2003. Neuregulins: functions, forms, and signaling strategies. Exp. Cell Res. 284, 14–30.

Fluck, C.E., Meyer-Boni, M., Pandey, A.V., Kempna, P., Miller, W.L., Schoenle, E.J., Biason-Lauber, A., 2011. Why boys will be boys: two pathways of fetal testicular androgen biosynthesis are needed for male sexual differentiation. Am. J. Hum. Genet. 89, 201–218.

Fujimoto, Y., Tanaka, S.S., Yamaguchi, Y.L., Kobayashi, H., Kuroki, S., Tachibana, M., Shinomura, M., Kanai, Y., Morohashi, K., Kawakami, K., Nishinakamura, R., 2013. Homeoproteins six1 and six 4 regulate male sex determination and mouse gonadal development. Dev. Cell 26, 416–430.

Garratt, A.N., Voiculescu, O., Topilko, P., Charnay, P., Birchmeier, C., 2000. A dual role of erbB2 in myelination and in expansion of the schwann cell precursor pool. J. Cell Biol. 148, 1035–1046.

Gu, Z., Eils, R., Schlesner, M., 2016. Complex heatmaps reveal patterns and correlations in multidimensional genomic data. Bioinformatics 32, 2847–2849.

Hacker, A., Capel, B., Goodfellow, P., Lovell-Badge, R., 1995. Expression of Sry, the mouse sex determining gene. Development 121, 1603–1614.

Hiramatsu, R., Matoba, S., Kanai-Azuma, M., Tsunekawa, N., Katoh-Fukui, Y., Kurohmaru, M., Morohashi, K., Wilhelm, D., Koopman, P., Kanai, Y., 2009. A critical time window of Sry action in gonadal sex determination in mice. Development 136, 129–138.

Hynes, N.E., Lane, H.A., 2005. ERBB receptors and cancer: the complexity of targeted inhibitors. Nat. Rev. Canc. 5, 341–354.

Jameson, S.A., Natarajan, A., Cool, J., DeFalco, T., Maatouk, D.M., Mork, L., Munger, S.C., Capel, B., 2012. Temporal transcriptional profiling of somatic and germ cells reveals biased lineage priming of sexual fate in the fetal mouse gonad. PLoS Genet. 8, e1002575.

Karl, J., Capel, B., 1998. Sertoli cells of the mouse testis originate from the coelomic epithelium. Dev. Biol. 203, 323–333.

Kim, D., Pertea, G., Trapnell, C., Pimentel, H., Kelley, R., Salzberg, S.L., 2013. TopHat2: accurate alignment of transcriptomes in the presence of insertions, deletions and gene fusions. Genome Biol. 14, R36.

Lecureuil, C., Fontaine, I., Crepieux, P., Guillou, F., 2002. Sertoli and granulosa cell-specific Cre recombinase activity in transgenic mice. Genesis 33, 114–118.

Li, L., Cleary, S., Mandarano, M.A., Long, W., Birchmeier, C., Jones, F.E., 2002. The breast proto-oncogene, HRGalpha regulates epithelial proliferation and lobuloalveolar development in the mouse mammary gland. Oncogene 21, 4900–4907.

Liu, C., Rodriguez, K., Yao, H.H., 2016. Mapping lineage progression of somatic progenitor cells in the mouse fetal testis. Development 143, 3700–3710.

Love, M.I., Huber, W., Anders, S., 2014. Moderated estimation of fold change and dispersion for RNA-seq data with DESeq2. Genome Biol. 15, 550.

Mendis-Handagama, S.M., Risbridger, G.P., de Kretser, D.M., 1987. Morphometric analysis of the components of the neonatal and the adult rat testis interstitium. Int. J. Androl. 10, 525–534.

Meyer, D., Birchmeier, C., 1995. Multiple essential functions of neuregulin in development. Nature 378, 386–390.

Meyer, D., Yamaai, T., Garratt, A., Riethmacher-Sonnenberg, E., Kane, D., Theill, L.E., Birchmeier, C., 1997. Isoform-specific expression and function of neuregulin. Development 124, 3575–3586.

Morohashi, K., Zanger, U.M., Honda, S., Hara, M., Waterman, M.R., Omura, T., 1993. Activation of CYP11A and CYP11B gene promoters by the steroidogenic cell-specific transcription factor, Ad4BP. Mol. Endocrinol. 7, 1196–1204.

Naillat, F., Veikkolainen, V., Miinalainen, I., Sipila, P., Poutanen, M., Elenius, K., Vainio, S.J., 2014. ErbB4, a receptor tyrosine kinase, coordinates organization of the seminiferous tubules in the developing testis. Mol. Endocrinol. 28, 1534–1546.

Nef, S., Verma-Kurvari, S., Merenmies, J., Vassalli, J.D., Efstratiadis, A., Accili, D., Parada, L.F., 2003. Testis determination requires insulin receptor family function in mice. Nature 426, 291–295.

Nel-Themaat, L., Vadakkan, T.J., Wang, Y., Dickinson, M.E., Akiyama, H., Behringer, R.R., 2009. Morphometric analysis of testis cord formation in Sox9-EGFP mice. Dev. Dynam. 238, 1100–1110.

Pitetti, J.L., Calvel, P., Romero, Y., Conne, B., Truong, V., Papaioannou, M.D., Schaad, O., Docquier, M., Herrera, P.L., Wilhelm, D., Nef, S., 2013. Insulin and IGF1 receptors are essential for XX and XY gonadal differentiation and adrenal development in mice. PLoS Genet. 9, e1003160.

Russell, L.D., Chiarini-Garcia, H., Korsmeyer, S.J., Knudson, C.M., 2002. Bax-dependent spermatogonia apoptosis is required for testicular development and spermatogenesis. Biol. Reprod. 66, 950–958.

Schmahl, J., Capel, B., 2003. Cell proliferation is necessary for the determination of male fate in the gonad. Dev. Biol. 258, 264–276.

Schmahl, J., Eicher, E.M., Washburn, L.L., Capel, B., 2000. Sry induces cell proliferation in the mouse gonad. Development 127, 65–73.

Schmahl, J., Kim, Y., Colvin, J.S., Ornitz, D.M., Capel, B., 2004. Fgf9 induces proliferation and nuclear localization of FGFR2 in Sertoli precursors during male sex determination. Development 131, 3627–3636.

Sekido, R., Lovell-Badge, R., 2008. Sex determination involves synergistic action of SRY and SF1 on a specific Sox9 enhancer. Nature 453, 930–934.

Shannon, P., Markiel, A., Ozier, O., Baliga, N.S., Wang, J.T., Ramage, D., Amin, N., Schwikowski, B., Ideker, T., 2003. Cytoscape: a software environment for integrated models of biomolecular interaction networks. Genome Res. 13, 2498–2504.

Sheean, M.E., McShane, E., Cheret, C., Walcher, J., Muller, T., Wulf-Goldenberg, A., Hoelper, S., Garratt, A.N., Kruger, M., Rajewsky, K., Meijer, D., Birchmeier, W., Lewin, G.R., Selbach, M., Birchmeier, C., 2014. Activation of MAPK overrides the termination of myelin growth and replaces Nrg1/ErbB3 signals during Schwann cell development and myelination. Genes Dev. 28, 290–303.

Shima, Y., Morohashi, K.I., 2017. Leydig progenitor cells in fetal testis. Mol. Cell.

Endocrinol. 445, 55–64.
Shima, Y., Miyabayashi, K., Haraguchi, S., Arakawa, T., Otake, H., Baba, T., Matsuzaki, S., Shishido, Y., Akiyama, H., Tachibana, T., Tsutsui, K., Morohashi, K., 2013. Contribution of Leydig and Sertoli cells to testosterone production in mouse fetal testes. Mol. Endocrinol. 27, 63–73.
Stallings, N.R., Hanley, N.A., Majdic, G., Zhao, L., Bakke, M., Parker, K.L., 2002. Development of a transgenic green fluorescent protein lineage marker for steroidogenic factor 1. Mol. Endocrinol. 16, 2360–2370.
Stevant, I., Neirijnck, Y., Borel, C., Escoffier, J., Smith, L.B., Antonarakis, S.E., Dermitzakis, E.T., Nef, S., 2018. Deciphering cell lineage specification during male sex determination with single-cell RNA sequencing. Cell Rep. 22, 1589–1599.
Tung, P.S., Skinner, M.K., Fritz, I.B., 1984. Cooperativity between Sertoli cells and peritubular myoid cells in the formation of the basal lamina in the seminiferous tubule. Ann. N. Y. Acad. Sci. 438, 435–446.
Umehara, T., Kawashima, I., Kawai, T., Hoshino, Y., Morohashi, K.I., Shima, Y., Zeng, W., Richards, J.S., Shimada, M., 2016. Neuregulin 1 regulates proliferation of Leydig cells to support spermatogenesis and sexual behavior in adult mice. Endocrinology 157, 4899–4913.
Wolpowitz, D., Mason, T.B., Dietrich, P., Mendelsohn, M., Talmage, D.A., Role, L.W., 2000. Cysteine-rich domain isoforms of the neuregulin-1 gene are required for maintenance of peripheral synapses. Neuron 25, 79–91.
Zhang, J., Eto, K., Honmyou, A., Nakao, K., Kiyonari, H., Abe, S., 2011. Neuregulins are essential for spermatogonial proliferation and meiotic initiation in neonatal mouse testis. Development 138, 3159–3168.
Zhou, B., Ma, Q., Rajagopal, S., Wu, S.M., Domian, I., Rivera-Feliciano, J., Jiang, D., von Gise, A., Ikeda, S., Chien, K.R., Pu, W.T., 2008. Epicardial progenitors contribute to the cardiomyocyte lineage in the developing heart. Nature 454, 109–113.